PEDOT:PSS for capacitive deionization

by

Xiangyu Lu

B.Sc., St Francis Xavier University, 2019

Thesis Submitted in Partial Fulfillment of the
Requirements for the Degree of
Master of Science

in the
Department of Chemistry
Faculty of Science

© Xiangyu Lu 2022
SIMON FRASER UNIVERSITY
Fall 2022

Copyright in this work is held by the author. Please ensure that any reproduction or re-use is done in accordance with the relevant national copyright legislation.

Declaration of Committee

Name:	**Xiangyu Lu**
Degree:	**Master of Science**
Title:	**PEDOT:PSS for capacitive deionization**
Committee:	**Chair: Charles Walsby** Associate Professor, Chemistry
	Loren Kaake Supervisor Associate Professor, Chemistry
	Jeffrey Warren Committee Member Associate Professor, Chemistry
	Hua-Zhong Yu Committee Member Professor, Chemistry
	Krzysztof Starosta Examiner Professor, Chemistry

Abstract

Capacitive deionization (CDI) is an energy efficient brackish water desalination technique which allows low voltage operation (~ 1.2V) under room temperature and pressure. Carbon material is the most studied material for CDI electrodes. However, the maximum salt adsorption capacity (MSAC) of carbon CDI have reached a limit (~20 mg/g). We have developed an in-situ CDI performance measurement system and tested the desalination performance of CDI cell with activated carbon electrodes and PEDOT:PSS electrodes. Conductivity change of solution inside our CDI cell was monitored during the desalination process. The dependence of salt adsorption on potential difference between CDI electrodes and feed water concentration have been investigated. We compared the desalination behavior of our all-polymer CDI cell with activated carbon and demonstrated that the two materials work under different physical principles. Most notably, the PEDOT:PSS cell has an MSAC that increases with salinity, suggesting its use in applications beyond the desalination of brackish water. An MSAC of over 55 mg/g have been obtained for our PEDOT:PSS CDI system in desalination of 10 g/L salt solution.

Keywords: PEDOT:PSS; Conductive polymer; Capacitive deionization; Faradaic electrodes

Acknowledgements

First and most, I would like to send my sincere gratitude to my senior supervisor Dr Loren Kaake. It has been really an adventure through out three years. Thank you for the consistent support and determination in the project, which motivates me all the way along. Second, I would like to thank my committee members Dr Jeffrey Warren and Dr Hogan Yu for providing insightful advice through out the project. I would also like to thank my group members for creating a friendly and supportive atmosphere in the office. I am grateful for having the opportunity working with people in Department of Chemistry, without the help from machine shop and electronic shop, this project would not go this far.

To my dearest family, we have been apart for almost 6 years. I really miss the days we were together having spring festival dinner. While you pray a good future for me every year, my biggest wish is to see you again sooner. To my brother, thank you for providing accompany when I was feeling down. To my closest friends Fangyu and Lelei, thank you for always being on my side and supported me through the hardest days, I feel blessed to meet you guys.

Finally, I would like to thank everything I have experienced, for building me today.

Table of Contents

List of Figures

List of Acronyms

3-ATES	3-Amimopropyltriethoxysilane
AC	Alternating Current
AEM	Anion Exchange Membrane
AFG	Arbitrary Function Generator
ASAR	Average Salt Adsorption Rate
BWRO	Brackish Water Reverse Osmosis
CDC	Carbide Derived Carbon
CDI	Capacitive Deionization
CE	Charge Efficiency
CEM	Cation Exchange Membrane
CN	Carbon Nanosheet
CNT	Carbon Nanotube
DC	Direct Current
DMAc	N,N-Dimethylacetamide
ED	Electrodialysis
EDL	Electrical Double Layer
FCDI	Flow Capacitive Deionization
GND	Ground
GOPS	3-Glycidoxypropyltrimethoxysilane
ICC	Isolated Closed Cycle mode
IEM	Ion Exchange Membrane
MCDI	Membrane Capacitive Deionization
MED	Multi-Effect Distillation
Mn	Number average molecular weight
MSAC	Maximum Salt Adsorption Capacity
MSF	Multi-Stage Flash distillation
NF	Nanofiltration
NP	Nanoparticle
OC	Open Cycle mode

OMC	Ordered Mesoporous Carbon
Op-amp	Operational Amplifier
PEDOT	Poly(3,4-ethylenedioxythiophene
PEI	Polyethyleneimine
PNDIE	Poly[N,N-(ethane-1,2-diyl)-1,4,5,8-naphthalenetetracarboxiimide]
PSQ	Polysilsesquioxane
PSS	Polystyrene sulfonate
PU	Polyurethane
PVDF	Polyvinylidene fluoride
RO	Reverse Osmosis
SAC	Salt Adsorption Capacity
SC	Single cycle mode
SCC	Short-circuited Closed Cycle mode
SFU	Simon Fraser University
SWRO	Sea Water Reverse Osmosis
TDS	Total dissolved solids

Chapter 1.
Introduction

1.1. Global water scarcity

Growing population and economy have increased water consumption around the world. **Figure 1.1** shows a historical trend of total annual water consumption around the world from 1900 to 2025.[1] The total annual withdrawal of freshwater increases at a dramatic speed, it is anticipated the total annual global water consumption would exceed 5000 m^3 in 2025.

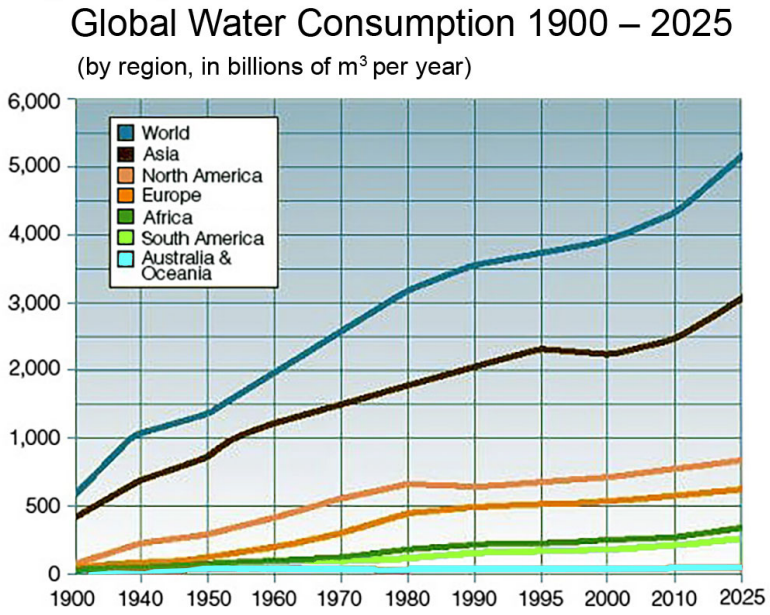

Figure 1.1. Historical trend of global water consumption per year (1900-2025) [1]

There are more than 2 billion people in the world that lack access to basic water. In middle Africa, serious water crisis results in food shortage and environmental refugees. Limited water resource also leads to frequent water conflicts between nations. As **figure 1.2** shows, amount of water conflicts happening per year is increasing from 1930 to 2017.[2] In 2017, 70 conflicts about water resources happened around the world. People dies not only because of water scarcity, but also because of the war caused by the scarcity.

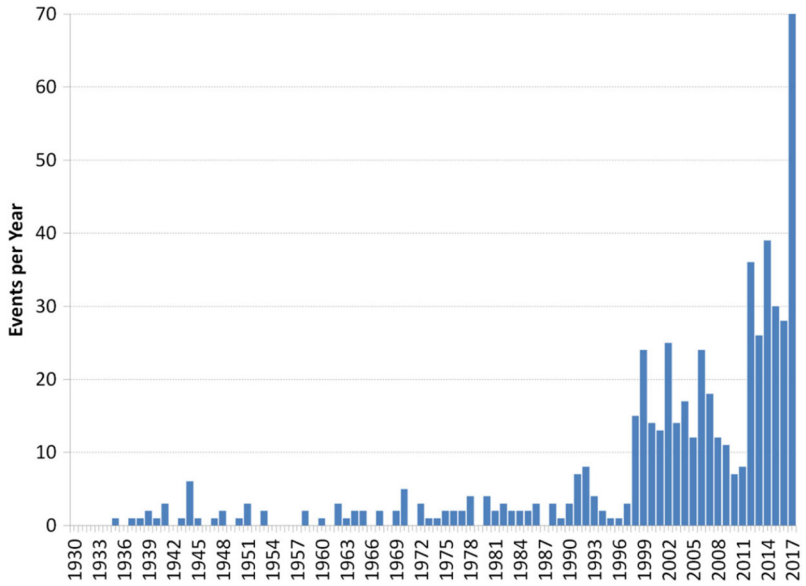

Figure 1.2. Water conflict events around the world per year from 1930 to 2017 [2]

As the demand for freshwater is increasing, freshwater resource on the Earth remains limited. Only about 2.5% of water in the world is freshwater, with most of the water resources stored as mountain glaciers or deep underground water. Due to global warming, mountain glaciers are melting every year (**Figure 1.3**)[3]. It can be anticipated that one thirds of glacier will disappear by the end of the century, which is a huge loss of freshwater. Water from melting glaciers flows into the ocean and increases the sea level, which further causes land freshwater to become salty, exacerbating global water scarcity. The object of our research is to address water scarcity by providing means for desalination.

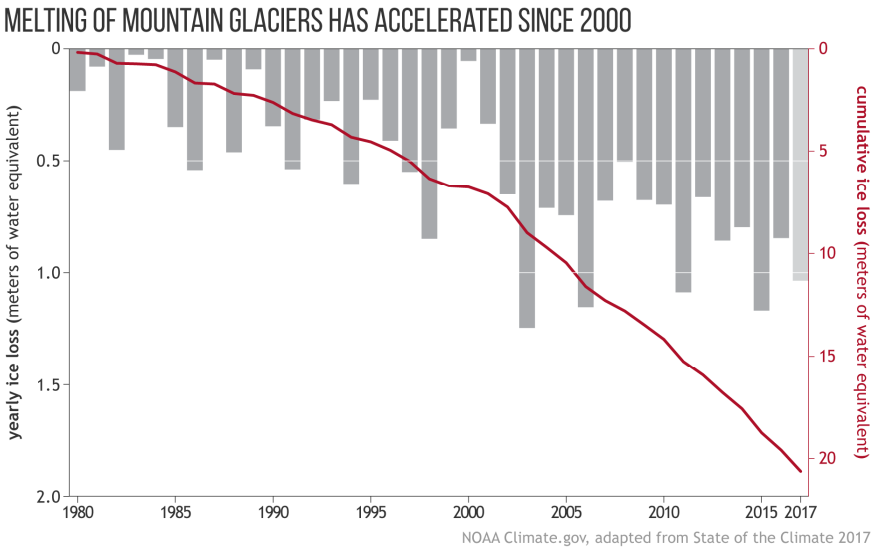

Figure 1.3 Melting of mountain glaciers from 1980 to 2017 [3]

1.2. Desalination techniques

Oceans have about 97% of water on the earth. However, sea water is salty and difficult to use in agriculture or industry. Desalination techniques have been developed to transform sea water into usable freshwater. The first desalination plants appeared in large number in late 1950s.[4] Low cost of fossil fuel made thermal desalination the most popular method in the first generation of desalination plants.[4] Fossil fuel price increases and social attention to carbon dioxide emission have pushed the development of more energy efficient desalination techniques. Desalination capacity describes the volume of desalinated water produced per year. By the year of 2018, Reverse Osmosis (RO) became the most popular technique of water desalination and contributed 69% of desalination capacity around the world, while multi-stage flash (MSF) and multi-effect distillation (MED) becoming popular, if secondary, desalination methods. (**Figure 1.4**) [5]

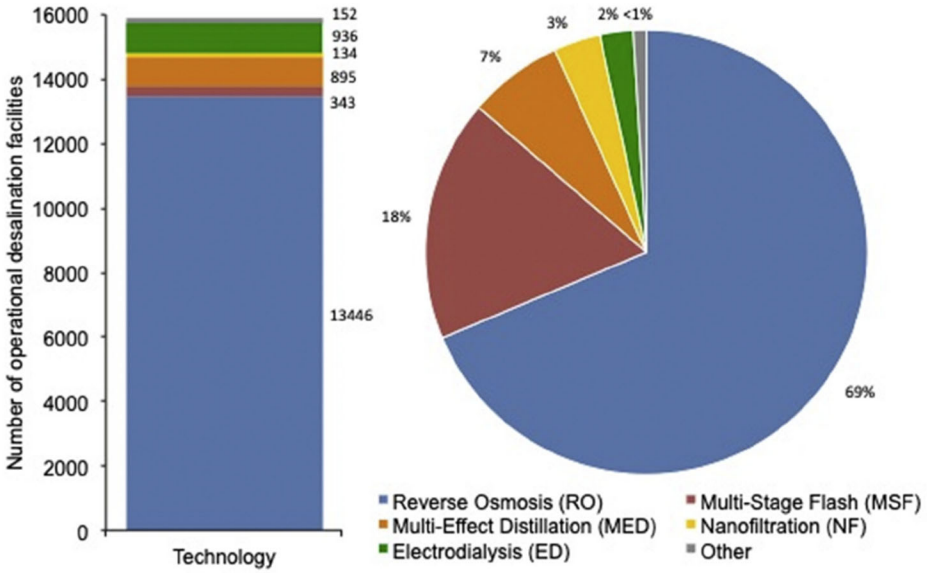

Figure 1.4 Number of operational desalination facilities (left) and desalination capacity (right) by technology (2018) [5]

This section will introduce the principles of current major desalination methods, in order to provide an idea of advantages and shortcomings of different desalination techniques.

1.2.1. Thermal desalination

Thermal desalination are desalination methods in which sea water is evaporated with thermal energy. Vaporized sea water then condensed on a surface that collects desalinated water. Multi-effect distillation (MED) and multi-stage flash distillation (MSF) are two important thermal desalination techniques currently, making up 25% of total desalination capacity of the world.

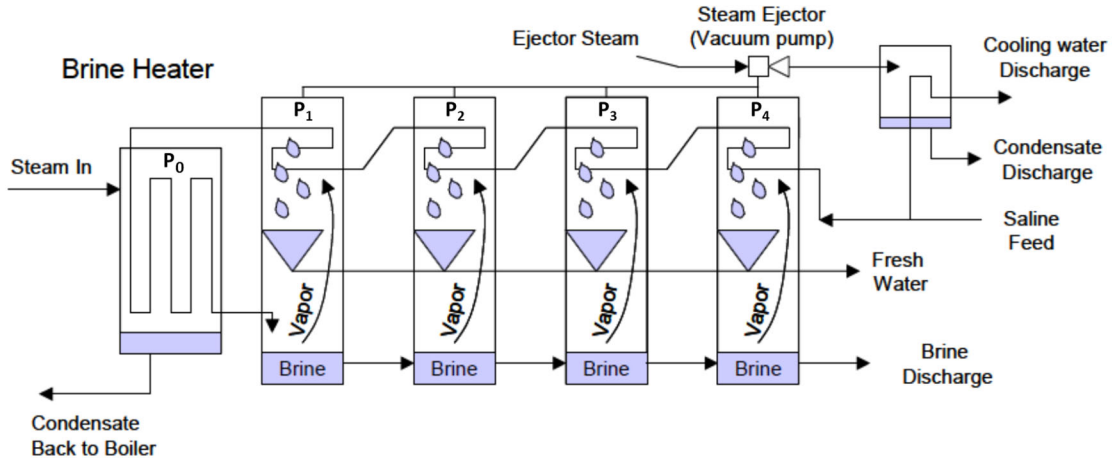

Figure 1.5 Schematic of multi-stage flash distillation process [6]

MSF is a technique based on flash evaporation of water. When boiling water in a high-pressure tank is transferred into a low-pressure tank, part of water evaporates to leave vapour and liquid phase in equilibrium. MSF includes a series of tanks with pressures varying from tank to tank from high to low pressures ($P_0 > P_1 > P_2 > P_3 > P_4$) (**Figure 1.5**)[6]. Feed saline water is boiled at pressure P_0 (about 2.5 bar)[7] then transferred to the first tank with pressure P_1. Because of the saline water is at higher temperature than the boiling point at P_1, part of saline water evaporates before being condensed by the feeding tube and collected by a collector. The rest of the saline water concentrates as brine in the bottom of the tank, it will be transferred to a tank with a lower pressure P_2, which causes a part of liquid vaporize again. Brine flows into series of tanks with decreasing pressure in MSF system. The multi-stage system provides an optimized use of heat comparing to direct flash distillation.

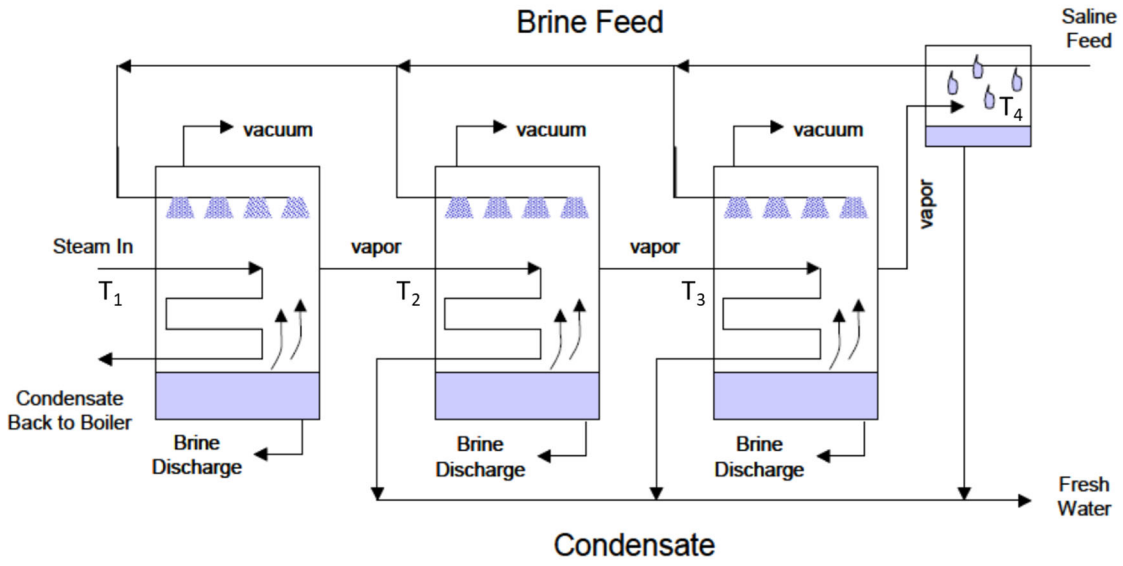

Figure 1.6 Schematic of multi-effect distillation process [6]

MED uses a similar multi-stage setup as MSF, but this setup relies more upon the temperature difference between stages instead of a pressure difference. As **figure 1.6** shows, saline water is feed into all the tanks with vapor tube. The vapor tube of first tank is supplied by vapor from boiler, while the vapor tube of other tanks is supplied by vapor from the previous tank. Vapor in the vapor tube boils the brine in the next tank producing vapor, this vapor again heats next tank and is eventually condensed as fresh water. However, because of heat loss between stages, the temperature of vapor used to heat each successive tank is decreasing ($T_1 > T_2 > T_3 > T_4$). The final temperature, T_4, would be the same temperature as environment, limiting the number of stages the MED system can have. This problem can be solved by connecting MED system with an adsorption desalination (AD) system, which allows a controllable ending temperature[8].

Thermal desalination is good for processing high salinity feed water into high quality freshwater. However, disadvantages like low recovery ratio (product vs feed) and corrosion caused by exposure of high temperature feed water of high salinity limits its overall application. Current high fossil fuel price also increases the cost of unit produced freshwater by thermal desalination plants. In addition, the system produces CO_2 through the burning of fossil fuels, further limiting its applicability as a sustainable solution to the problem of freshwater production.

1.2.2. Reverse osmosis (RO)

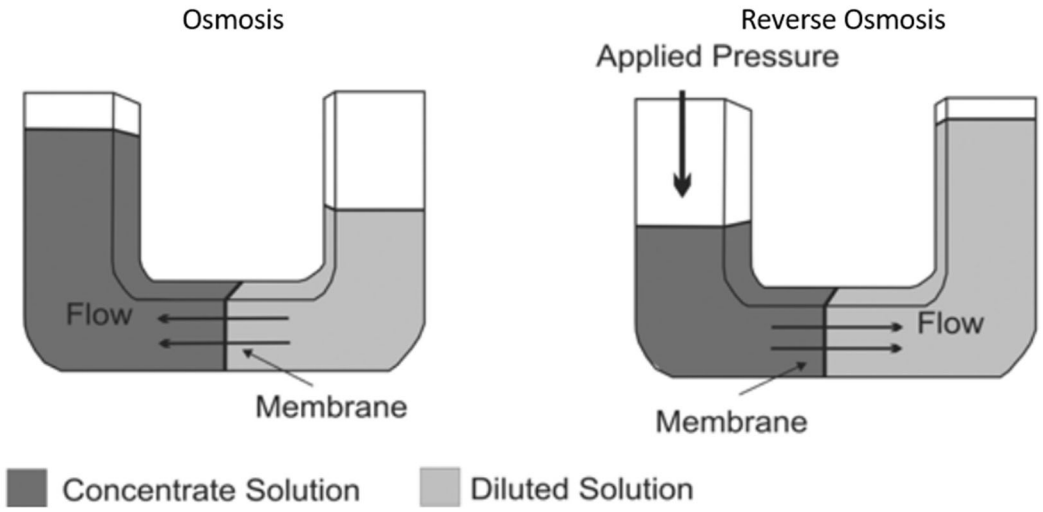

Figure 1.7 Schematic of reverse osmosis principle [9]

Reverse osmosis (RO) is currently the most popular and most state-of-art technique for processing brackish water. The principle of RO is based on a semi-permeable membrane which only passes water molecules. As **figure 1.7** shows, when a concentrated solution and a diluted solution are separated by the semi-permeable membrane, water molecule will pass through the membrane from diluted solution to concentrated solution via the process of osmosis. By applying a pressure on the concentrate solution side (feed pressure), water molecule can pass the membrane from concentrate solution to diluted solution. Semipermeable membranes used in RO system are often thin film polyamide composites.[10]

The average salinity of sea water is 35 g/L while salinity of industrial brackish water is normally lower than that level. Based on the salinity of feed water treated by RO, RO systems have been separated into brackish water RO (BWRO) and seawater RO (SWRO). The distinction is necessary as each feed stream requires different optimization conditions, and different considerations to prevent membrane fouling. SWRO have a wide range of acceptable feed water concentrations, as required by the salinity of ocean. While BWSO usually works with feed water salinity from 1 g/L to 10 g/L.[11] The membranes used in SWRO are required to be more impermeable to NaCl than that of BWRO. This consideration also lowers the flux of fresh water, as well as lowering the recovery ratio of SWRO relative to BWRO.[12]

Membrane fouling is problem for all RO systems. Due to membrane fouling, a membrane replacement is required every 2-5 years for SWRO and 5-7 years for BWRO. Fouling on RO membrane increases the required pressure on concentrated water feed, and negatively influences the permeate freshwater quality. In addition to challenges with respect to fouling, RO suffers from relationship between water recovery rate and feed pressure. High pressures are required (15-25 bar for BWRO, 54-80 bar for SWRO)[13], reducing the energy efficiency of the technique. As a result current research on RO focus on reducing membrane fouling and improving energy efficiency.[12]

1.2.3. Electrodialysis (ED)

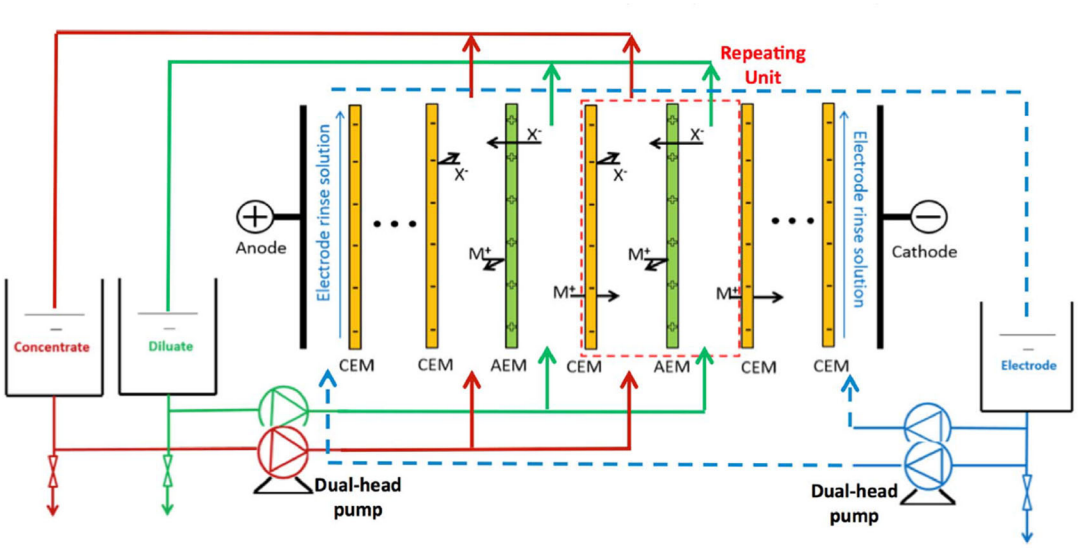

Figure 1.8 Schematic diagram of electricdialysis setup [14]

Electricdialysis has been considered as a safe and environmentally friendly desalination method comparing to thermal desalination and RO. The operation of ED system does not require heat or pressure, electricity is directly used for desalination process. **Figure 1.8** shows the principle of ED system. Cation exchange membranes (CEM) and anion exchange membranes (AEM) are stacked between negative electrodes and positive electrodes, while feed water flows in the space between CEMs and AEMs. Because of the electric potential on Positive electrodes and negative electrodes, counter ions are attracted and flow towards them. Cations would pass CEM but get stopped by AEM, while anions would pass AEM but get stopped by CEM. With separation of AEM and CEM, feed water is separated into dilute phase and concentrate phase. Dilute phase is collected as product while concentrated phase is fed back into the ED system for further

desalination. To prevent poisonous chlorine formation near the electrodes, dilute $Na_2(SO_4)$ solution is used to rinse the electrodes.[15]

Feed concentration controlling is important for optimizing working condition of an ED system. ED system works best at a moderate feed concentration range (0.4-6 g/L).[15,16] High concentration feed water accelerates membrane fouling, while the low conductivity of low concentration feed water reduces ED energy efficiency.

In addition, membrane fouling is also a primary issue in ED systems. Fouling of ion exchange membranes would lower exchange efficiency and increase electric resistance. Feed water pre-treatment for removing organic impurities and maintaining moderate salt concentration is necessary in an ED system to reduce membrane fouling.

1.3. Capacitive deionization (CDI) basics

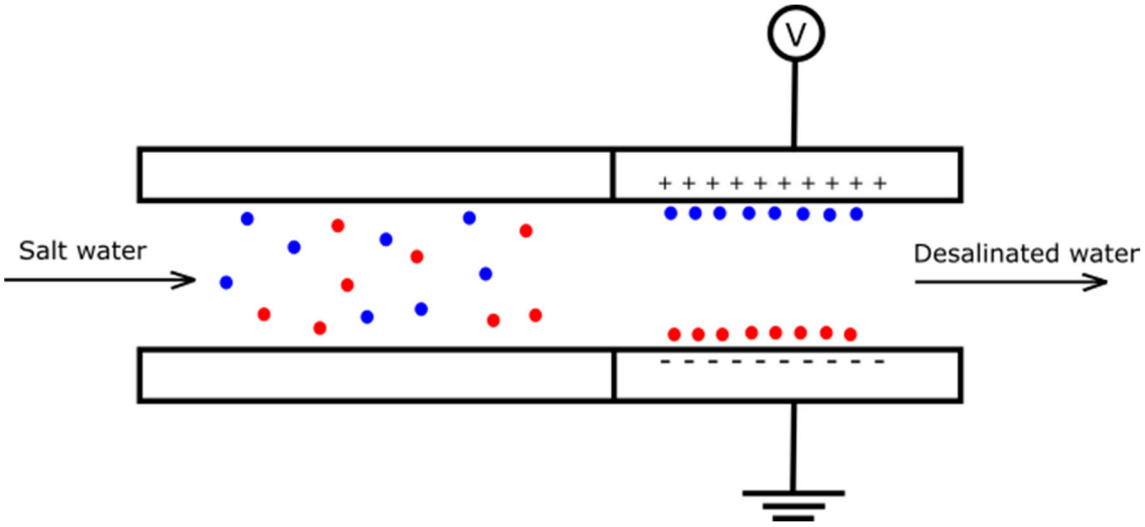

Figure 1.9 Schematic diagram of capacitive deionization working principle

Capacitive deionization (CDI) is believed to be an energy efficient process that has the potential to compete with other techniques of desalination. This is due to the fact that the molarity of NaCl molecules in unit volume of sea water, is way lower than that of water molecules. Therefore, it is more efficient to remove salt ions from the feed stream than water molecules. As an example of industrialized CDI system, ESTPURE have build a CDI plant in China desalinates brackish water from total dissolved solids (TDS) level of 1 g/L to 0.25 g/L, produces 10000 tons desalinated water per day.[17]

Similar to ED systems, CDI systems can also operate under room temperature and pressure. CDI system is driven by an electric potential applied between two electrodes. As feed water flows between the electrodes, salt ions are adsorbed on their surface (**Figure 1.9**). During this process, the feed water is desalinated until the electrodes become saturated with salt. To remove the salt, a brine stream is created by passing feed water through the CDI system with no potential applied to the electrodes. The electrodes will then release salt ions into the cleaning stream, releasing their stored energy in a manner similar to a supercapacitor. This electrical energy can be reused to charge another set of electrodes, making CDI a potentially high efficiency desalination technique.

Advantages like high recovery ratio and low energy consumption make CDI a promising desalination technique for the next generation. However, low energy efficiency in feed water with high TDS due to co-ion expulsion and organic fouling limit the performance of CDI desalination devices.[18] In order to provide a clear view of CDI technique, electrical double layer theory and important metrics for evaluating CDI performance are introduced in the following section.

1.3.1. Electrical double layer

In an ideal CDI system, every electron passed as current to the electrodes would accumulate, result in a counter-ion firmly attracted to the electrode surface. The ratio between the moles of electrons passed to the electrodes and the moles of salt ions removed from solution is called charge efficiency (CE) with and ideal CE reaching unity. However, in practice, CDI systems are not perfectly efficient due to the complicated behavior of ions around a charged surface.

Electrical double layer (EDL) model has been developed to describe the structure of attracted ions around a charged surface in ionic solution. Herman von Helmholtz[19] first realized the existence of double layer on charged surface in ionic solution and developed first model of this layer. In the Helmholtz model, surface charges are directly compensated by a layer of counter-ions attached firmly to the surface, while co-ions are repelled away from the surface. This model considers ions as point charge and the approach of ions towards electrodes are unlimited, while size effect of counter-ions is ignored in the model. This causes problem when explaining different adsorption of ions with same charge but different size[20].

The Helmholtz model gives a basic view of ion attraction on the electrode surface, but it does not include the factor of counter-ion diffusion in the solution. Gouy-Chapman model of EDL considers the idea that the layer of attracted counter-ions is not as compact as in Helmholtz model. In this model, attracted counter-ions form a diffuse layer near the electrodes, and are not firmly attached to the surface.

Otto Stern[21] has further optimized the model by combining Gouy-Chapman model with Helmholtz model. In Gouy-Chapman-Stern theory, attracted counter-ions are separated into a Stern layer and diffuse layer. Attracted ions are firmly attracted to the electrode surface in the Stern layer, while ions diffuse in the solution in diffuse layer. Surface potential decreases linearly with the distance from ion-electrode interface in the Stern layer and follows exponentially decaying behavior in the diffuse layer. (**Figure 1.10**) The finite size of counter-ions limits the number of counter-ions in the Stern layer. Besides ion size, the number of counter-ions in the Stern layer is determined by the surface area of electrode, as well as the voltage applied to the electrode. According to X-ray photoelectron spectroscopy study of EDL on SiO_2 electrode surface in NaCl solution, thickness of the stern layer is around 0.6 to 0.9 nm, while diffuse layer has thickness of 3-4 nm.[22]

In CDI system, counter-ions forms EDL near the electrodes. Ions in the stern layer stays with electrode as adsorbed salt, while ions in diffuse layer leave the system together with the desalinated product.

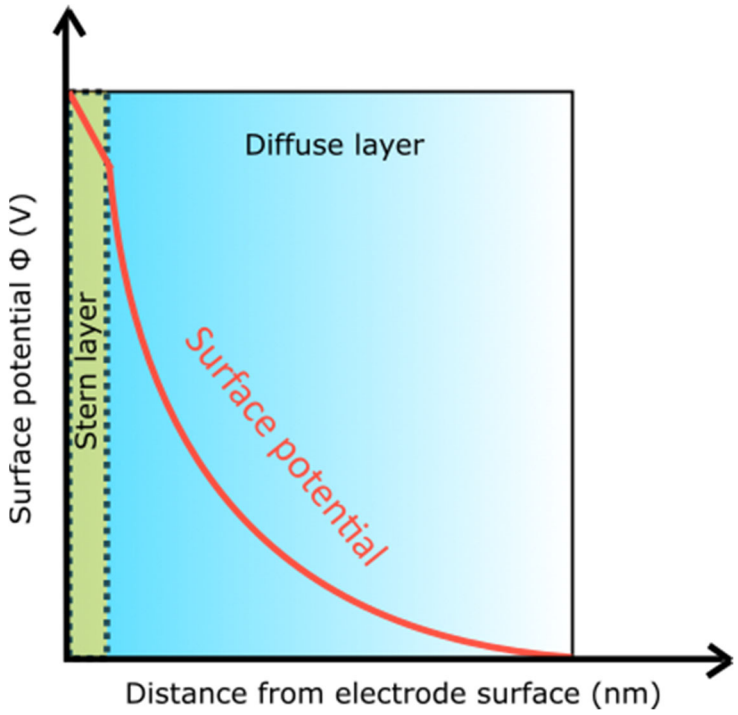

Figure 1.10 Schematic diagram of electric double layer according to the Gouy-Chapman-Stern theory

1.3.2. Important metrics

Since the concept of CDI desalination was originally developed in 1960,[23] metrics have been created for describing CDI system performance. Early research on the technique of CDI reported the reduction feed stream concentration under constant voltage charging.[24–26] However, feed stream concentration reduction can be influenced by system factors like mass of electrodes and flow rate of the stream. Without controlling for these system-based factors, it is possible for a highly effective system to be judged poorly as exhibiting a low feed stream concentration reduction. In order to more accurately demonstrate the performance of a CDI cell, metrics like salt adsorption capacity (SAC), average salt adsorption rate (ASAR) and CE have been developed and are commonly reported in many articles describing the effectiveness of a particular CDI cell.

SAC is a widely used metric for describing electrode performance in CDI system. It describes the amount of salt adsorbed by unit amount of electrode material. Maximum salt adsorption capacity (MSAC) is the SAC under fixed applied voltage at equilibrium. Measuring MSAC requires a long charging-discharging cycle of a pair of electrodes such that concentration of ions near electrodes can reach equilibrium. When MSAC is reached,

the concentration of feed stream across the CDI electrodes no longer changes. Calculation of MSAC can be done by dividing mass of salt removed by the mass of electrodes, giving the result in $mg \cdot g^{-1}$ (milligram of salt removed by gram of electrode material) (**Equation 2.1**).It should be noted that when counting electrode mass, all solid ingredient in both of CDI electrodes should be included (e.g., activated carbon and binder)[27].

$$MSAC\ (SAC) = \frac{mass\ of\ absorbed\ NaCl}{mass\ of\ elecrodes} \quad \textbf{2.1}$$

MSAC is a very useful metric because under fixed operational condition MSAC is a material property only related to the electrodes and would not be affected by other CDI system components. It is therefore an important metric to use when judging the effectiveness of a new CDI electrode material.

While MSAC provides a view of maximum amount of salt that is possible to get adsorbed by electrodes, ASAR provides another dimension of information: how fast salt can be adsorbed by the electrodes. ASAR can be calculated by dividing SAC by the time of full charging-discharging cycle (**Equation 2.2**), the unit is $mg \cdot g^{-1} \cdot min^{-1}$.

Comparing to MSAC, ASAR is more a system property than a material property. Many factors in CDI system can affect ASAR. For example, shorter charging time would result in a higher ASAR since the adsorption rate is fastest in the beginning. Higher feed water concentration would allow more rapidly charging, which also increases the ASAR.

$$ASAR = \frac{SAC}{full\ cycle\ time} \quad \textbf{2.2}$$

It is meaningless comparing ASAR across different CDI systems when their operational factors are different. However, since an optimized ASAR can be reached in a CDI system when specific operation factors are controlled, indicating the metric is useful when optimizing a CDI system during use in a real-world application.

Different from MSAC and ASAR, CE is an important metric for evaluating energy cost in the desalination process. CE can be calculated by dividing moles of salt adsorbed by moles of charge passed as current into the CDI cell (**Equation 2.3**).

$$CE = \frac{moles\ of\ NaCl\ absorbed}{moles\ of\ charge} \qquad \textbf{2.3}$$

Theoretically, a mole of charge accumulated on the electrodes would result in a mole of ion removed from solution. However, in practice, not all the charge on the electrodes necessarily contributes to salt adsorption. As **Figure 1.11** shows, given a fixed amount of energy per ion removed, a higher CE would naturally result in lower energy consumption.

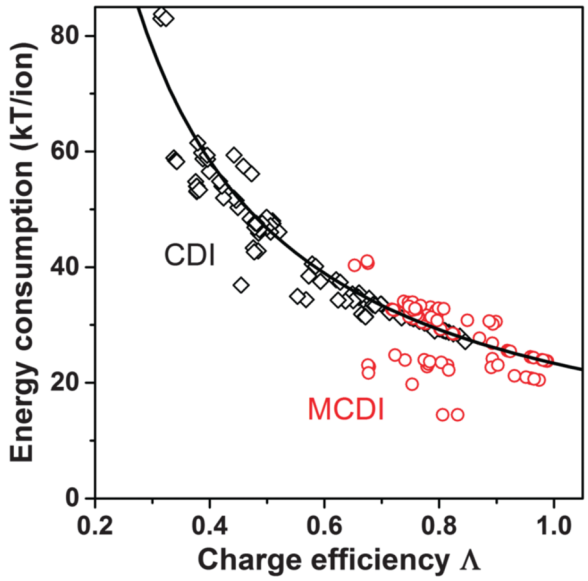

Figure 1.11 Data for energy consumption per ion vs charge efficiency based on reported CDI and MCDI data operated under different conditions [27,28]

1.4. CDI system design

To optimize the desalination performance of a CDI system, a variety of configurations have been developed. For example, studies optimizing system geometry, applying ion-exchange membranes, and flow electrode designs has pushed the development of next generation CDI plants. Good CDI design would allow system to have a high desalination rate and high energy efficiency. This section introduces several CDI system designs as well as their advantages and disadvantages.

1.4.1. Cell Geometries of CDI system

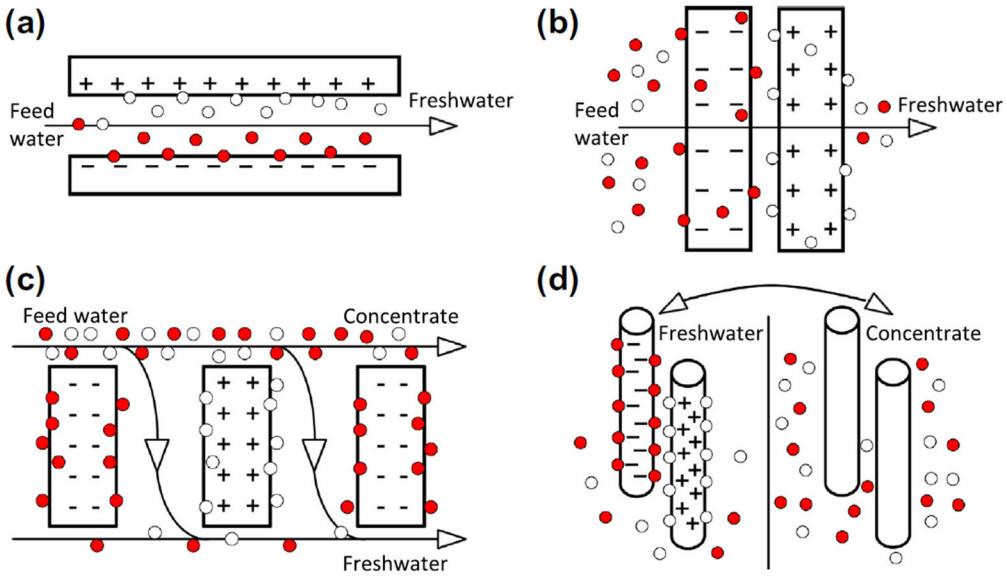

Figure 1.12 Common cell geometries of CDI system. Red and white dots represents sodium and chloride ions, respectively.[29] a) flow-by mode b) flowthrough mode c) electrostatic ion pumping mode d) wire CDI mode

Figure 1.12 shows different geometries of CDI system. Flow-by mode is the classic CDI cell geometry in which two electrodes are set parallel to each other with an open channel between them where the feed stream can flow (**Figure 1.12a**). In a flow-by mode CDI cell, electrodes can either be free standing electrode material, or coated films on current collectors. Due to easy construction and space saving of the design, flow-by mode remains the most used CDI cell geometry in application.

Another competing cell geometry is flow-through mode developed by Newman and Johnson in 1970.[30] In this geometry, water is pumped through the layered porous electrodes with a flow direction perpendicular to their surface (**Figure 1.12b**). In order to reduce the required pressure for water to pass through the cell and increase energy efficiency, a larger pore size (diameter ~ 10 um pore with 10nm micropores) comparing to [i]flow-by mode (diameter < 100 nm) is required.[31] Compared to flow-by mode, flow-through mode has the advantage of a fast adsorption rate since ions are in closer proximity to the surface of electrodes when solution flowing through them. However, Faradaic process[1]

[1] Faradaic process: Redox reactions associated with charge transfer

between unwanted compounds (e.g. organic pollutant) and electrodes happens more frequently in flow-through CDI cell, with electrode oxidation further exacerbating Faradaic reactions between electrode and ions, undermining both the MSAC and charge efficiency of flow-through CDI cell.[32]

When a CDI cell reaches its MSAC, electrodes need to be discharged to remove adsorbed salt so that it can continue desalinating in a new charging cycle. The discharge process of the electrode would increase the salt concentration in the feed stream and produce brine. In flow-by mode and flow-through mode, product from charging (freshwater) and discharging (brine) exit the cell from the same place, which may cause contamination of freshwater produced. Changing feed stream flow direction may be a way to solve the problem. Electrostatic ion pumping mode CDI cell is a geometry which allows brine and freshwater to have different exits from the cell, avoiding the contamination at the switch of electrodes charging state. In electrostatic ion pumping mode CDI, there are two pathways for feed water to flow through the cell, one is for freshwater exit the cell (pathway A) and the other is for brine exit the cell (pathway B). During charging, pathway B is closed, feedwater passes through pathway A to get desalinated. During discharging, pathway A is closed, brine pass through pathway B to wash adsorbed salt from electrodes (**Figure 1.12c**).

Another geometry separates brine and freshwater is wire CDI. In wire CDI, electrodes are made into wires or thin rods. During charging, feed stream is desalinated to produce freshwater. When discharging, wire electrodes are removed from the feed stream and immersed into another stream to release salt (**Figure 1.12d**). This CDI geometry would allow the entire production process of freshwater and brine to occur in different parts of the cell, thus avoiding contamination from the sequence charging and discharging. Also, since reduction of the electrode is accomplished in another stream, uninterrupted desalination of feed water can be done with multiple wire CDI systems.

1.4.2. Membrane CDI (MCDI)

Porous carbon is the most common electrode material for CDI system. When porous carbon is immersed into feed stream, there will be both cations and anions adsorbed in the pores of the electrodes in the absence of applied voltage. This is the initial state of the electrode. **Figure 1.13** shows the charge compensation in the electrode pores

when charge is accumulated on the electrodes. In the initial state of porous carbon electrode in NaCl solution where no voltage has been applied, both anions and cations can enter the pores of electrodes. When charging starts, counter-ions are adsorbed by electrodes while co-ions in the pore are expelled from the electrodes at the same time. Co-ions expulsed from electrodes cause the concentration of salt to increase in the bulk solution during desalination process, lowering the charge efficiency of the CDI system.

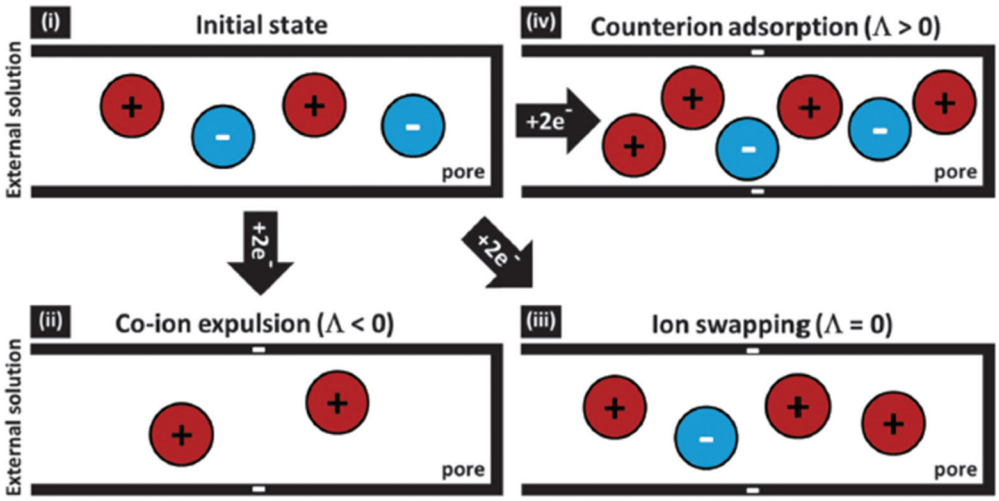

Figure 1.13 Fundamental electrical charge compensation mechanisms from i) initial state to ii) co-ion expulsion (CE < 0) iii) ion swapping (CE = 0) iv) counter-ion adsorption (CE > 0) [27]

To improve charge efficiency, ion exchange membranes (IEM) have been introduced in CDI system, in a process called membrane CDI (MCDI). Common MCDI system includes an anion exchange membrane (AEM) and a cation exchange membrane (CEM) placed in front of positive electrodes and negative electrodes respectively (**Figure 1.14**). IEM in front of the electrodes prevents co-ion from entering the pores of electrodes, which eliminates the influence of co-ion expulsion. Therefore, comparing to traditional CDI systems, MCDI systems have improved MSAC and CE.

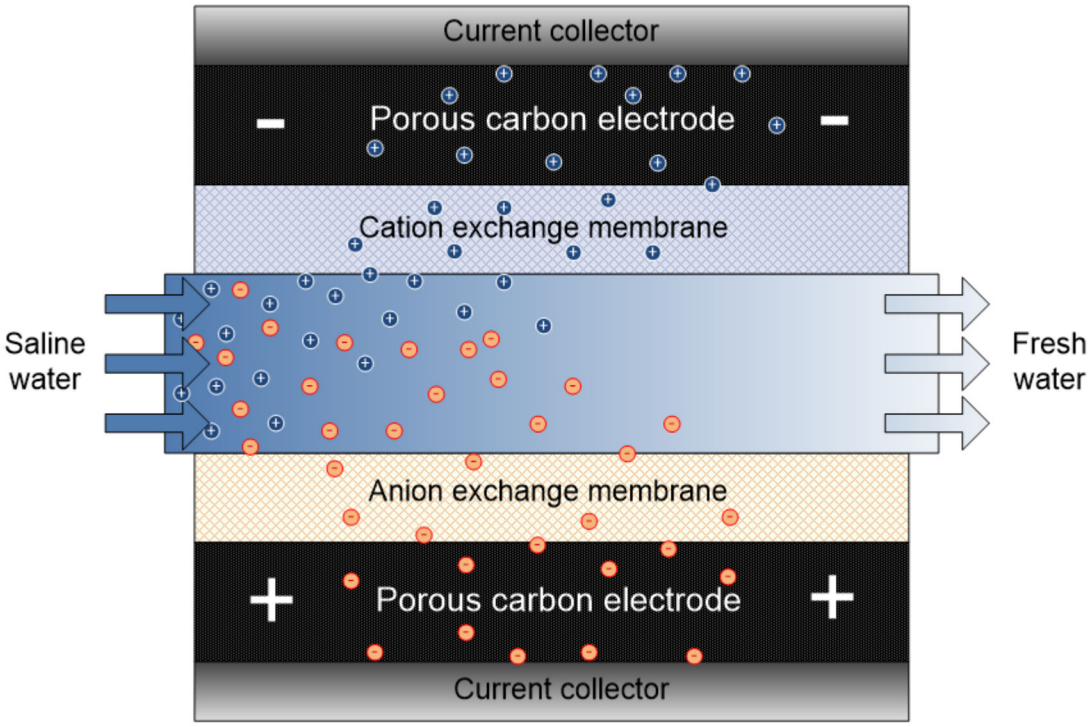

Figure 1.14 Schematic diagram of typical MCDI system [33]

In real application of CDI systems, dissolved organics in feed water could be a problem. Fouling caused by bonding of dissolved organics to the electrode would increase the energy consumption of CDI system and reduce salt removal. Application of membranes provides a protection for the electrode surface, preventing electrodes from being deactivated by fouling compounds. Hassanvand et al. compared the desalination performance between CDI and MCDI system in presence of humic acid and sodium alginate as foulant, showing a more stable performance of MCDI system than CDI system.[34]

MCDI system have also been studied for selective ion removal for different ions. Water softening is an example of selective ion removal in application. Due to the existence of Na^+, the adsorption efficiency of Ca^{2+} is undermined as Na^+ occupies some active sites on electrode surface. Ion adsorption in MCDI system can be divided into two steps. Ions are firstly adsorbed by ion exchange membranes. In the second step, ions adsorbed on membranes would move to the surface of electrodes. Because the electrodes can only adsorb ions which have passed through the membranes, ion selective removal can be realized by chemically adjusting the ionic preferences of the ion exchange membrane. For the application of water softening, Nnorom et al. have found MCDI system with sulfonated

ion exchange membrane coated on carbon electrodes have a high selectivity (6.0 ± 1.5) towards Ca^{2+} over Na^{+}. The Ca^{2+}/Na^{+} selectivity of sulfonated membrane coated electrodes is much improved compared to carbon electrodes without membrane coating (2.9 ± 0.7), which allows an effective water softening process with MCDI setup.[35]

1.4.3. Flow electrode CDI (FCDI)

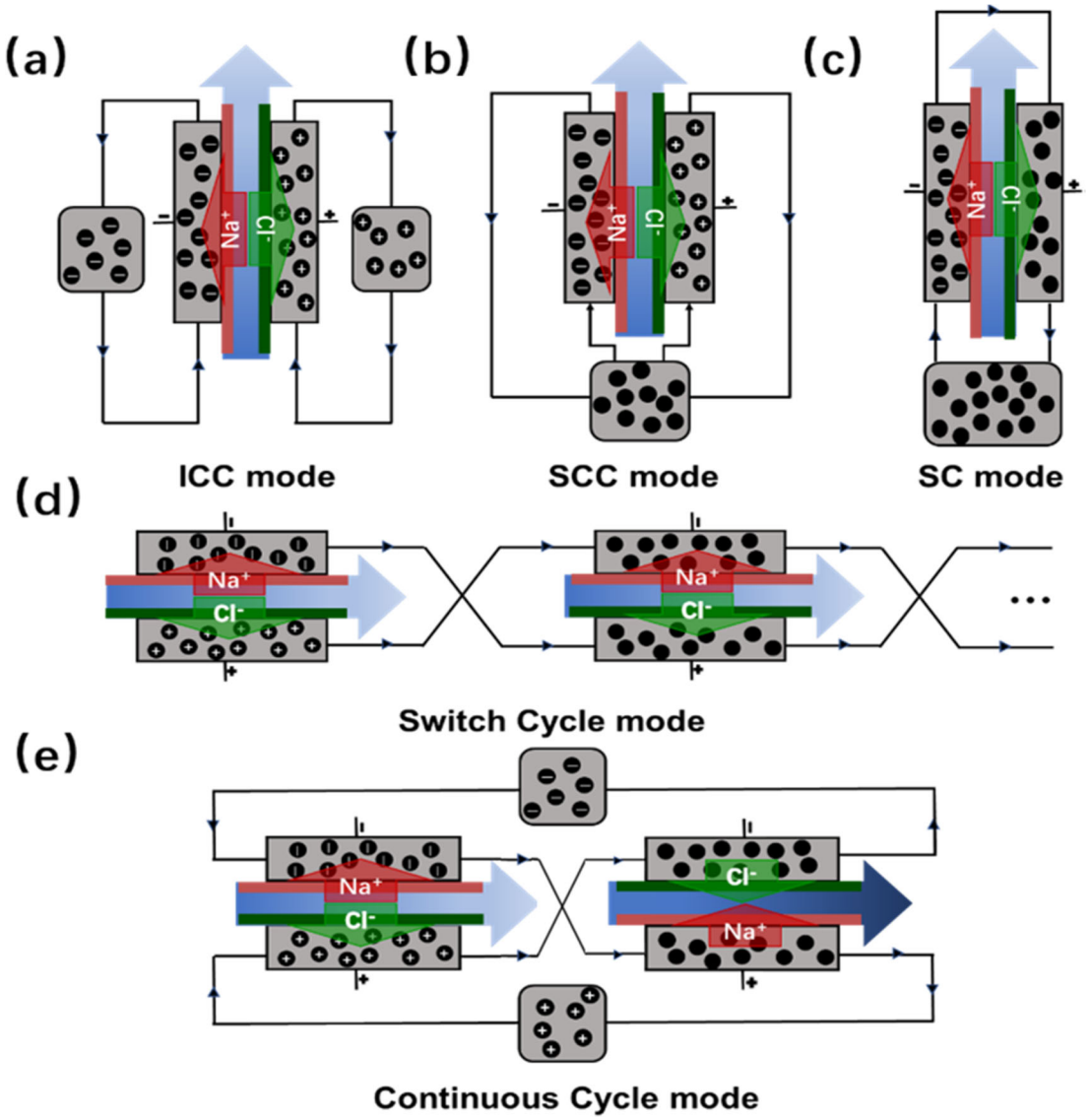

Figure 1.15 **Schematic diagram of different configurations of FCDI system [36] (a) isolated closed cycle mode (ICC) (b) short-circuited closed cycle mode (SCC) (c) single cycle mode (SC) (d) switch cycle mode (e) continuous cycle mode**

The application of ion exchange membranes can reduce co-ion adsorption and expulsion in CDI system, improving the desalination efficiency of electrodes. However, electrode saturation remains a problem in all fixed electrode CDI systems. When electrodes are saturated with adsorbed ions, no more ions can be adsorbed as there are no active sites for ions to attach. A discharge process for releasing ions is required to restore electrodes, which would interrupt the desalination process.

Flow electrode CDI (FCDI) has been invented based on MCDI systems.[37] In contrast to MCDI systems, FCDI systems use flowing suspended activated carbon as the electrode material. The electrode slurry flows through the channel curved on the current collector with ion exchange membrane separating flowing electrode slurry from feed water. Since electrode material is flowing by the CDI cell, electrodes are not saturated during charging. Without the necessity of discharging the electrodes, continuous desalination can be realized with FCDI system. Flowing electrode also allows easy scale up of the process achieved by increasing volume of flowing electrode material.

The configuration of FCDI system have profound influence on desalination efficiency of FCDI system. FCDI systems can be divided into single module configuration and multiple module configuration. In single module configurations, CDI units are independent to each other, flow electrode does not transfer between CDI units. In multiple module configurations, the flowing electrode material travels through all CDI units in the system.

The first model of FCDI systems operate in open cycle (OC) mode, in which infinite electrode material flows by the current collectors. Assuming an infinite reservoir of flowing electrode material, OC mode FCDI system have infinite salt adsorption capacity, but the cost of maintaining a continuous flow of electrode material is huge. Closed cycle modes appear more practical. Isolated closed cycle mode (ICC) (**Figure 1.15a**) and short-circuited closed cycle (SCC) (**Figure 1.15b**) modes are the main configurations of closed cycle mode. The only difference between ICC and SCC is that ICC separates positive electrodes and negative electrodes circulation, while SCC have a total reservoir for circulating positive electrodes and negative electrodes. Comparison between ICC and SCC mode have shown that ICC electrode easily get saturated during desalination just as fixed electrode CDI systems, while SCC has a constant salt removal rate since salt ions

are recombined and released in the total reservoir where positive electrodes and negative electrodes material mixes.[38]

Besides ICC and SCC mode, SC mode is a novel configuration in which negative electrodes material with adsorbed ions directly pumped into positive electrodes continues adsorbing counter ions while adsorbed ions are released forming concentrated brine (**Figure 1.15c**). Ion exchange membranes prevent mixing between brine and feed in SC mode. This configuration not only simplifies the construction of cell, but also helps ion release from charged electrodes, which improve the desalination efficiency.

Multiple module configurations include switch cycle mode (**Figure 1.15d**) and continuous cycle mode (**Figure 1.15e**). In switch cycle mode, electrode slurry flows through CDI units alternatively in positive electrodes and negative electrodes. Adsorbed cations and anions in the electrode slurry during desalination are released into concentrated brine. Ion exchange membranes separate feed water and brine near the electrode surface so that continuous salt adsorption is realized. Continuous cycle mode reverses the position of ion exchange membranes in an alternative CDI unit allowing the flowing electrode slurry to take the same route as in switch cycle mode. In more detail, the flowing electrode slurry adsorb salt in the first CDI unit, then release ions in the second CDI unit. Continuous mode does not require a periodic electrode restoring process as in other configurations, allowing for a continuous desalination process. More generally, both multiple module configurations give high desalination efficiency and reduced energy consumption while providing continuous desalination.

1.5. CDI Electrode materials

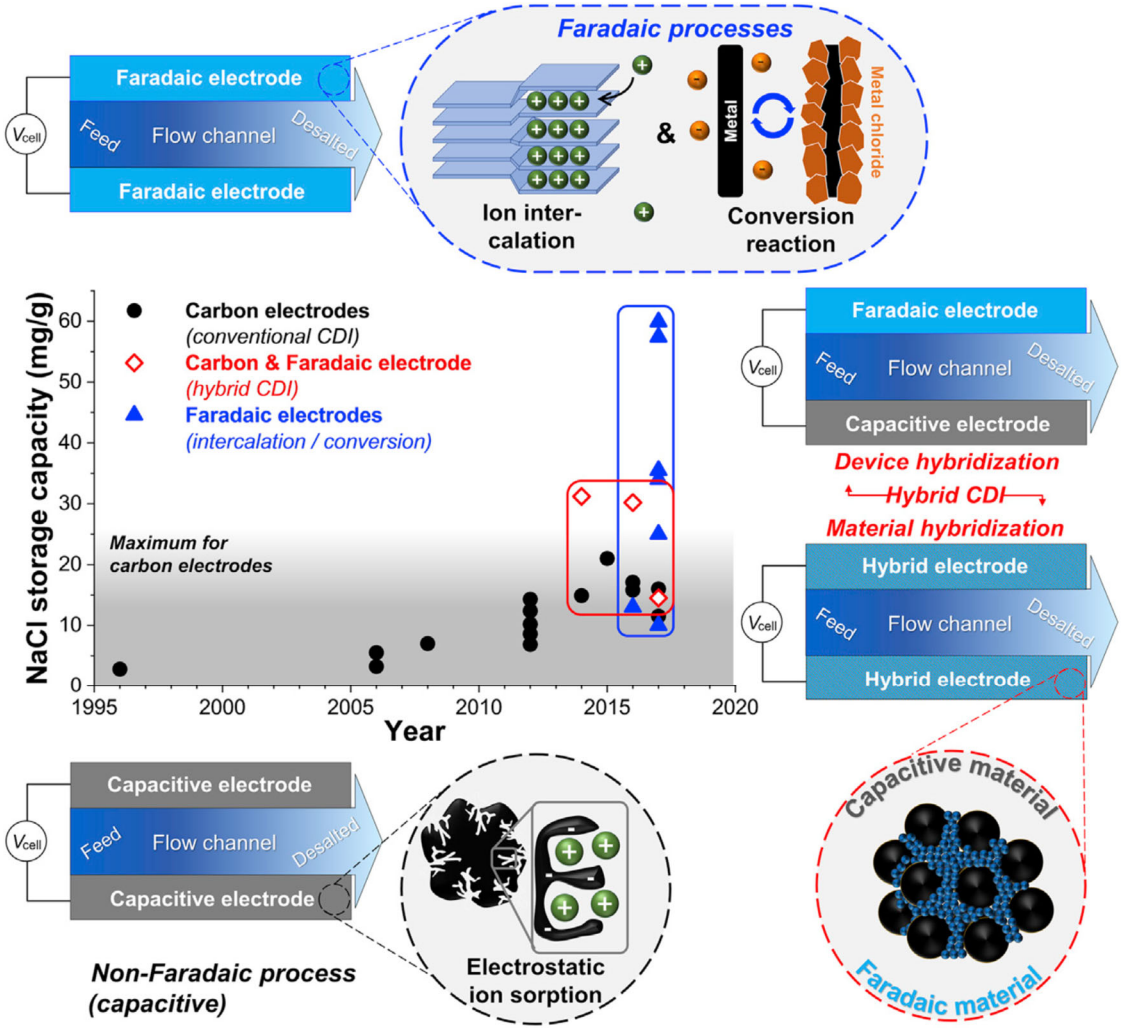

Figure 1.16 Mechanisms schematic diagrams and reported MSACs for conventional CDI, hybrid CDI and Faradic CDI systems [39]

Besides configuration of CDI system, electrode material is also an important factor affecting CDI performance. CDI electrode materials can be divided into capacitive electrodes and Faradaic electrodes. With capacitive electrodes, desalination is based on formation of EDL by adsorbed counter-ions. While in Faradaic electrodes, the Faradaic reaction between ions in the solution and electrode material provides the salt removal capacity in a manner resembling a lithium-ion battery.

Conventional CDI systems utilizing two capacitive electrodes is currently the most used configuration. Studies upon optimizing conventional CDI systems are reaching a plateau showing that the MSAC of a conventional system is limited to approximately 20

mg/g. To further improve performance of CDI system, Faradaic electrodes have been developed for CDI applications. Instead of EDL from electrostatic ion adsorption, reversible Faradaic reactions like ion intercalation and conversion are the mechanisms of ion adsorption on Faradaic electrodes. Research on hybrid CDI systems and pure Faradaic CDI systems has shown outstanding MSAC comparing to conventional electrodes. (**Figure 1.16**)

This section will introduce properties and desalinating mechanisms of different CDI electrodes, to provide contrasting viewpoints regarding the development of CDI electrode materials.

1.5.1. Capacitive electrodes

Salt removal by capacitive electrodes is based on surface EDL formed by adsorbed counter-ions. In order to have larger ions adsorption on electrode surface, a larger electrode surface area is favourable for good CDI performance. Besides large electrode surface area, high chemical stability over used pH and voltage, high electric conductivity and good wetting behaviour are also desired properties for good capacitive electrodes.

Activated carbon is the first and most used material in CDI systems due to its low cost (~0.5 $ per kg) and high surface area (1000-3500 m^2/g).[29] Conventional preparation of activated carbon includes pyrolysis step and activation step. In pyrolysis step, natural carbon precursors (like wood, coconut shell) are pyrolyzed under 600-800 Celsius in inert atmosphere to eliminate non-carbon components and produce char. In activation step, produced char is physically activated by gasification with steam or CO_2, or chemically activated by strong acids or bases.[40] MSAC for activated carbon CDI cells are around 6 mg/g.[41]

Porous carbon material can give large electrode surface area. With same porosity, smaller pore size theoretically results in larger surface area of an electrode. However, CDI performance is not directly related to surface area, large macropores may cause more counter-ions in diffuse layer, while small size of micropores may prevent ions from entering inner spaces.[42,43] Therefore, optimizing pore size and structure is necessary for carbon-based electrodes to increase ion accessible surface area.

Pore diameter of activated carbon electrodes varies from less than 2 nm to larger than 50 nm, indicating pore size and structure are not well controlled. Carbide-derived carbon (CDC) is a carbon material that allows an atomic porosity control during synthesis. The synthesis of CDC is based on removing metal atoms from metal carbide precursor with an etchant (dry chloride) in an elevating temperature (200-1000 Celsius), leaving behind the carbon material with controlled pore according to metal component. Pore size and structure can be controlled by adjusting the metal component in metal carbide precursor. Porada et.al. reported for the first time using CDC as CDI electrodes, and also shown that CDC with controlled micropore (less than 2 nm) has a higher charge efficiency and salt adsorption (~ 12 mg/g) than activated carbon.[44]

Ordered mesoporous (diameter 2-50 nm) carbon (OMC) has drawn intention since Zou et.al found mesoporous material facilitates ion adsorption on electrode surface.[45] Similar to CDC, the synthesis of OMC requires template material for pore size control. Silica-based template material mixed with carbon-based polymer or resin is the carbon precursor for OMC synthesis. The mixture is carbonated under high temperature (~ 800 Celsius) then HF processed to remove template material and leave behind mesoporous structure. Giannelis et.al. have developed hierarchical porous carbon structure (**Figure 1.17**) with micropores inside of mesopores,[46] demonstrating a fast salt removal rate (0.2 $mg \cdot g^{-1} \cdot min$) at a high salt adsorption capacity (~ 13 mg/g). Zhao et.al have built a 3D hierarchical porous carbon structure with self blowing technique ($KHCO_3$ as blowing agent mixed with resin will release gas during calcination) and obtained 17.83 mg/g as MSAC in 0.5 g/L NaCl solution with 1.2 V charged.

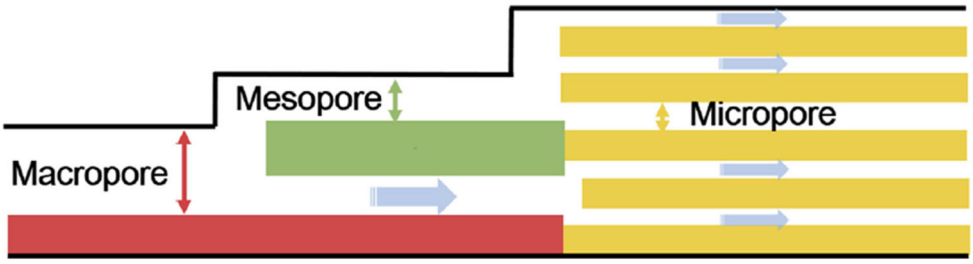

Figure 1.17 Schematic diagram of hierarchical porous carbon structure.[42] Micropore provide large surface area, while mesopore facilitate counter-ion transfer from macropores to micropores

Graphene is a sp^2 bonded 2D structural carbon-based material (**Figure 1.18b**). High electrical conductivity and chemically inertness have made graphene a promising

material for CDI application.[47] The open interlayered structure of graphene provides short access for counter-ions to diffuse into the electrodes, which facilitates counter-ion adsorption and desorption.[48] Carbon nanotube (CNT) is made up of a graphene sheet roll into a nanosized tube, thus having a similar covalent bond network as graphene (**Figure 1.18a**). The nanotube structure provides CNT extra mechanical strength and electronic conductivity.[49] Li et.al. have tested the CDI performance of pristine graphene and CNT reported salt adsorption of CNTs (0.74 mg/g and 0.55 mg/g for single walled CNT and double walled CNT) and graphene (0.46 mg/g).[50] The adsorption performance of pristine graphene and CNT suffers from aggregation. Aggregation cause irregular pore size and low surface area, which limits salt adsorption during CDI process.[51] Shi et.al. induced H_2O_2 in reduction of graphene oxide to prevent aggregation of produced graphene, obtained a 3D structure of interconnected graphene and reported an MSAC of 17.1 mg/g at applied voltage of 1.6 V.[52] Zhang et.al. produced homogenous CNT electrode by electrophoretic deposition with optimized electric field preventing aggregation and obtained 23.93 mg/g as MSAC.[53]

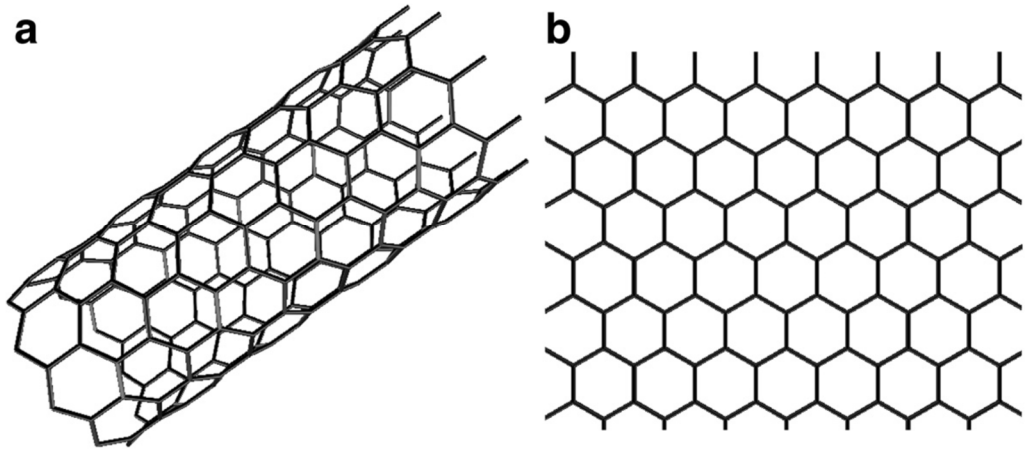

Figure 1.18 Structure of a) carbon nanotube b) graphene [54]

Doping heteroatoms onto carbon materials have also been developed as a strategy for improving CDI performance of the carbon electrodes. Nitrogen doped carbon material have been reported having good charge transfer ability and improved wettability, as well as increased porosity.[55,56] However, the reported salt adsorption improvement from singly nitrogen doping is limited (SAC ~10 mg/g). Multiple heteroatoms doping on carbon material has drawn attention not only because doping of heteroatoms increases number of active sites for ion adsorption, but also multiple heteroatoms doping have synergistic

catalytic effect accelerating oxidation reduction reaction between electrode and electrolyte, which increases capacitive performance.

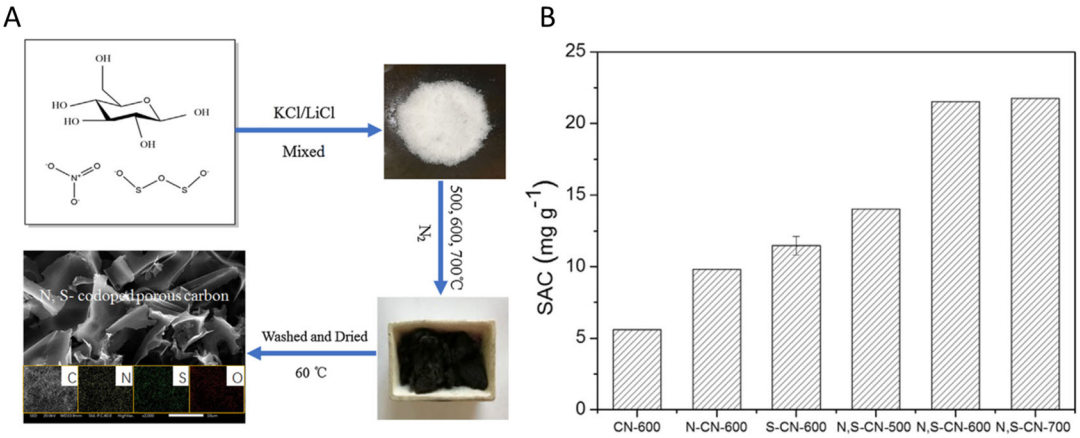

Figure 1.19 A) Procedure of preparation of porous carbon nanosheet with different dopant B) SAC of different carbon nanosheet (CN) in 80 mg/L NaCl solution. Number after CN is carbonization temperature [57]

Min et.al. prepared N,S co-doped porous carbon nanosheets as CDI electrodes, as well as singly N-doped and S-doped carbon nanosheets for comparison.[57] D-glucose was used as carbon precursor, while $Na_2S_2O_3$ and $LiNO_3$ was respectively used as sulfur source and nitrogen source. KCl/LiCl powder was used as porogen in this procedure to provide porosity. Carbon precursor, heteroatom source, and porogen was firstly mixed and homogenized, then carbonized with heating rate 5 °C/min at 600 °C for 2 hr under nitrogen atmosphere. Carbonized sample was washed with deionized water to remove porogen, then dried under 60 °C for 24 hrs to give the final product (**Figure 1.19A**). N,S co-doped carbon nanosheets have higher SAC than singly doped carbon nanosheets, showing that synergistic catalytic effect between nitrogen and sulfur improves CDI performance. Besides dopants, carbonization temperature is also an important factor that affects SAC (**Figure 1.19B**). An MSAC of 55.79 mg/g was reported by this study in 330 mg/L NaCl solution under 1.4 V applied potential.[57]

1.5.2. Faradaic electrodes

High theoretical MSAC and low energy consumption has made Faradaic electrode a popular direction for developing new generation CDI plants. Ion attraction on Faradaic electrode is based on charge transferring Faradaic reaction between electrode and ions, thus Faradaic CDI does not have co-ion expulsion problem. Faradaic reaction between

ions and electrode can happen in the bulk of electrode material, thus surface area is not a limiting factor for Faradaic electrode. Common mechanisms applied for Faradaic CDI includes (1) intercalation reactions, (2) conversion reactions, (3) electrolyte charge compensation, (4) ion-redox active moiety interaction (**Figure 1.20**).

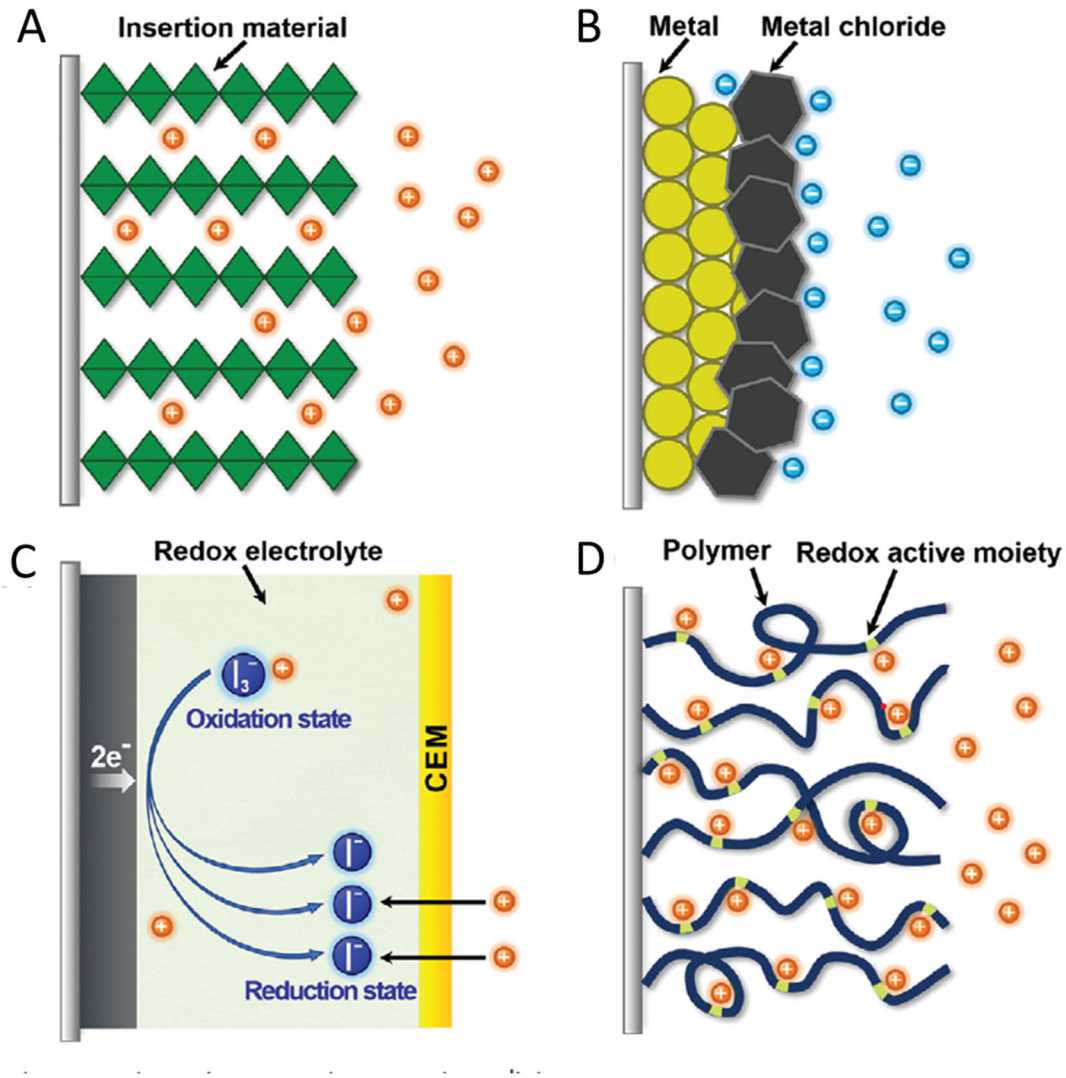

Figure 1.20 Schematic diagram of ion attraction mechanisms in Faradaic electrodes: A) Intercalation reaction B) convertion reaction C) electrolyte charge compensation D) ion-redox active moiety interaction [58]

Intercalation reaction is a process where ion insert into vacant sites in host material via charge transfer between ion and host material (**Figure 1.20A**). An ideal intercalation

material should have abundant space for ion insertion. Intercalation materials can be divided into 1D, 2D and 3D insertion materials according to different spatial dimension for ion insertion (**Figure 1.21**). 1D insertion materials (e.g., $Na_{0.44}MnO_2$)[59] have tunnel like channels for ion diffusion and storage in the material. 2D insertion materials (e.g., sodium vanadium oxides, MXenes)[60,61] have layered structures, where ion insertions happen within the interlayer space. 3D insertion materials (e.g., NASICON-type phosphates)[62] have open 3D framework structure, providing 3D transport channel help transferring ions to specific crystal structural sites for insertion. Ion insertion into vacant spaces within the material may cause structural change of material, increasing the distance between interlayers in 2D insertion materials, which causes capacity of electrodes to adsorb ions to decay during continuous desalination cycles.[63] In order to solve problems associated with structural changes during ion insertion, materials with a 3D open porous structure have been developed. Cao et.al. combined 3D open-structured $Na_3V_2(PO_4)_3$@C with commercial activated carbon as hybrid CDI system, obtained a high salt adsorption of 137.2 mg/g in 100mM NaCl solution.[62]

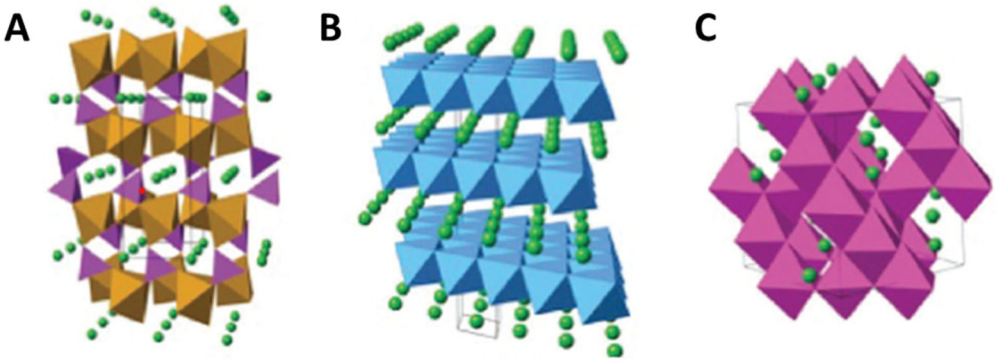

Figure 1.21 Schematic diagram of A) 1D B) 2D C) 3D insertion materials. Green particles represents inserted ions [64]

In conversion electrodes the reaction between electrode material and ion forms a new compound on electrode (**Figure 1.20B**). Conversion reaction material normally have high theoretical adsorption capacity. However, the conversion reaction between ion and electrode causes tremendous volume expansion of electrode, which makes electrode unstable. The low reaction rate of conversion reaction also makes achieving ideal CDI performance difficult.[58] Nam and Choi have built a MCDI system using a Bi electrode as positive electrodes and a BiOCl electrode as negative electrodes.[65] Chen et.al. combined a sodium manganese oxide insertion positive electrodes and a BiOCl conversion negative

electrodes into a Faradaic CDI system, and obtained a reversible salt adsorption rate of 68.5 mg/g.[59]

Electrolyte charge compensation is a mechanism in which salt ions do not directly reacts with electrode material, but instead react with redox electrolyte near electrodes through IEM. Example is shown in **Figure 1.20C**, I_3^- adsorbs 2 e^- and reduces into 3 I^- during electrodes charging. During the reduction, 2 Na^+ passed through the CEM into I_3^-/I^- electrolyte to balance the charge in the electrolyte solution. Lee et.al have built the CDI system with porous carbon material and iodide electrolyte separated from NaCl solution with IEM, and obtained a MSAC of 69 mg/g throughout 120 desalination cycles showing a highly stable desalination performance in feed concentration range of 17-600 mM (seawater concentration is around 600 mM). This mechanism is similar to electrodialysis method. Therefore, the quality of IEM is important for high CDI performance and preventing electrolyte solution polluting product.

Ion redox active moiety reaction is the desalination mechanism for redox active polymer CDI electrodes (**Figure 1.20D**). Redox reaction between ions in feed water and active moieties results in desalination of feed water. Redox active polymers can be divided into two groups according to the redox active moiety position: 1) redox active moiety suspended polymer, and 2) redox active moiety embedded polymer.

In redox active moiety suspended polymer (e.g., polyimide, polyquinone)[66,67], redox active moieties are connected to non-conductive backbones. Li et.al. synthesized a redox active polyimide, poly[N,N-(ethane-1,2-diyl)-1,4,5,8-naphthalenetetracarboxiimide] (PNDIE), as sodium adsorber combined with activated carbon electrode, and built a hybrid CDI system.[66] Carbonyl group connected to the polymer backbone are the active sites for sodium adsorption during charging, and this process can reverse during natural discharging (no applied voltage) (**Figure 1.22**). This hybrid CDI system provided a MSAC of 54.2 mg/g calculated for total mass of PNDIE and AC electrodes.

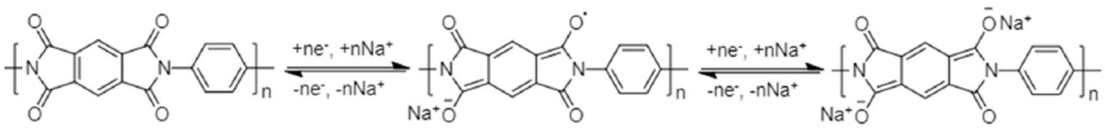

Figure 1.22 Schematic diagram for redox mechanism of PNDIE [68]

Redox active moiety embedded polymers have redox active backbones with active monomers (e.g., polypyrrole and polyaniline)[68,69]. Conjugated conductive polymers are typical redox active moiety embedded polymers. The π-conjugated double bonds of polymer backbone can be either p-doped with anions or n-doped with cations to maintain electrical neutrality, like polypyrrole (**Figure 1.23**). High electrical conductivity and fast charge transfer along conjugated backbone also made conjugated conductive polymer attractive for CDI application. Wang et.al have developed a CDI cell with CNT coated with polypyrrole modified by dodecyl benzyl sulfonate as Na^+ adsorber and a graphite cloth as Cl^- adsorber, and obtained a MSAC of 93.68 mg/g.[70] They have also synthesized polypyrrole/polyaniline composite, provided a uniform nanorod morphology with abundant mesopores. This composite is combined with carbon nanotube to form CDI cell, giving MSAC of 197.8 mg/g.[71]

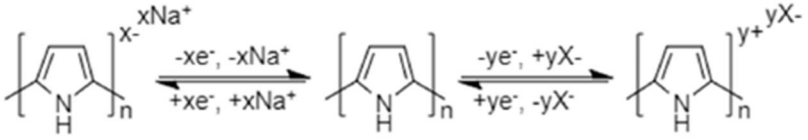

Figure 1.23 Schematic diagram of p-doping and n-doping reactions of polypyrrole [68]

Ion capture preference of polymers can be modified by adding redox active moieties on the backbone. For example, by doping sulfonate group onto polypyrrole backbone, the modified polypyrrole electrode would prefer interacting with Na^+ than Cl^-.[72] Silambarasan et.al have implanted $[Fe(CN)_6]^{4-}$ as redox active compound into polysilsesquioxane (PSQ) chain to make redox PSQ electrode.[73] This redox PSQ electrode have superior Cl^- adsorbing performance over conversion electrodes like Ag and Bi electrodes. Addition of redox group on polymer electrodes allow optimization of CDI performance by adjusting preference of ion interaction. Highly sodium preferred material combined with a highly chloride preferred electrode promises an excellent CDI performance.

1.6. PEDOT:PSS as CDI electrodes

Poly(3,4-ethylenedioxythiophene) (PEDOT) is a polymer (**Figure 1.24A**), that when polymerized in the presence of poly(styrene sulfonate) (PSS) (**Figure 1.24B**),

creates a stable, conductive, water-soluble suspension (PEDOT:PSS) that is perhaps the strongest example of a commercially successful conductive polymer (**Figure 1.25**).[74] The material is also of strong contemporary research interest as a transparent conductor,[75] a thermoelectrically active semimetal,[76] a biosensor,[77] and a neuromorphic computing element.[78] PEDOT:PSS transports both electrons and ions, and is heavily p-doped in its as-received form. The material can be cross-linked to create a water insoluble film that typically transports cations when cycled towards negative electrochemical potentials. It is found that the electrical conductivity of PEDOT:PSS generally increases with increasing PEDOT relative to PSS. Stocker et al. have demonstrated that PEDOT:PSS ratio of 1:1 has the highest conductivity while ratio of 1:30 have the lowest.[79] Thus, the conductivity of PEDOT:PSS can be optimized for different applications by controlling the ratio between PEDOT and PSS.

We demonstrate here that PEDOT:PSS can be used as an electrode for capacitive deionization, and that treatment with $CaCl_2$ allows it to transport anions. As a result, PEDOT:PSS can serve as both electrodes, thus demonstrating an all-polymer CDI cell. We compare the desalination behavior of our all-polymer cell with activated carbon and demonstrate that the two materials act on different physical principles. Most notably, the PEDOT:PSS cell has an MSAC that increases with salinity, suggesting its use in applications beyond the desalination of brackish water, the most common CDI application for activated carbon electrodes.

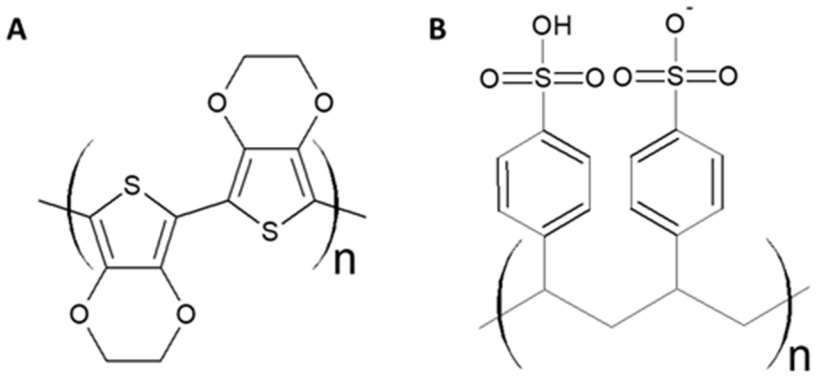

Figure 1.24 Chemical structure of (A) PEDOT (B) PSS

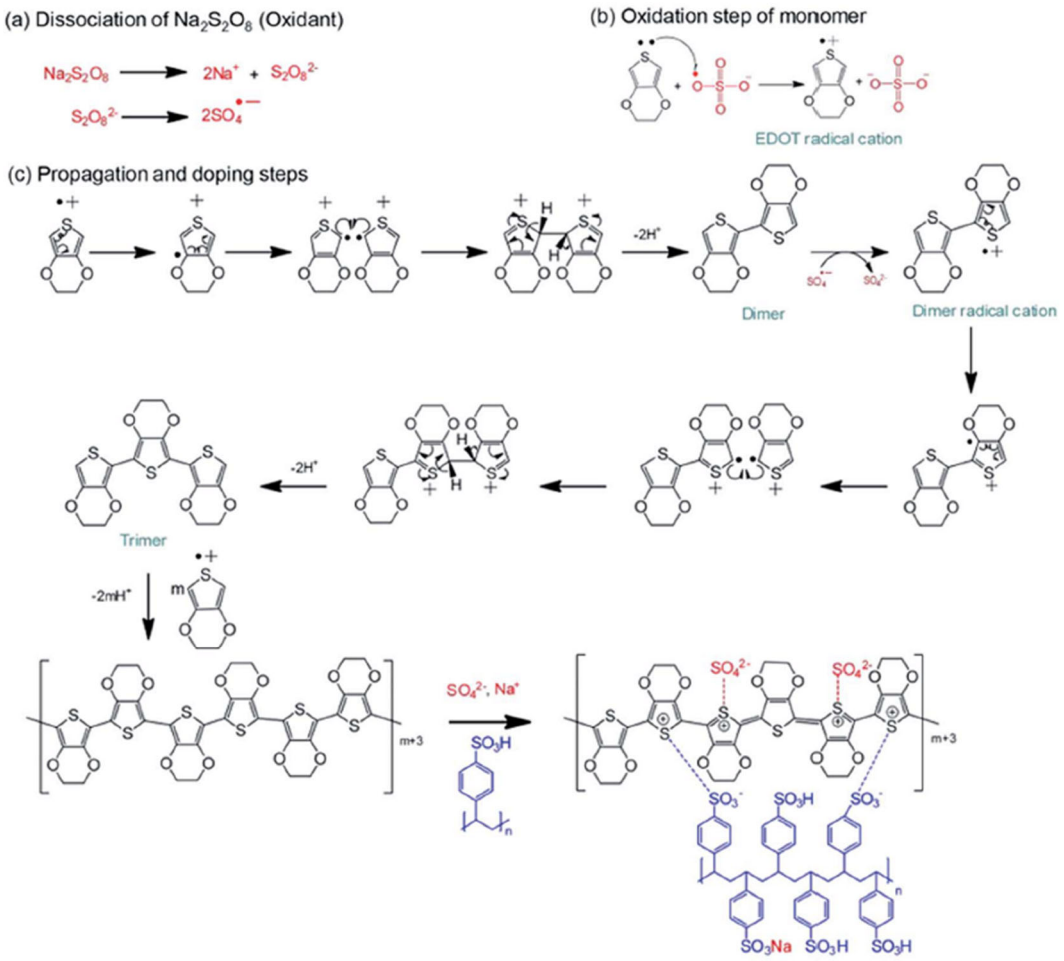

Figure 1.25 Mechanism of polymerization of PEDOT:PSS [74]

Chapter 2.
Experimental

2.1. In-situ solution concentration measurement

In order to collect in-situ measurements of capacitive deionization behavior, we created a custom 6 electrode electrochemical cell. This circuit allows us to simultaneously measure the electrical input to the capacitive deionization electrodes as well as the in-situ salt concentration during the deionization process. The equipment consists of two function generators, a two-channel transimpedance amplifier, a two-channel analog to digital converter, a lock-in amplifier, and custom current source. This section will describe the components in detail along with basic op-amp circuit design, in order to provide a clear explanation of the choices made during the design and testing process.

2.1.1. Solution conductivity

Electrical conductivity (σ) is a property that describes how easily a material conducts electric current. In aqueous electrolyte solution, electrical conductivity results from movement of positive and negatively charged ions. Pure water is known to have a resistance of 18.2 MΩ due to autoionization at neutral pH. However, this concentration is negligible as compared to the NaCl concentrations measured here. Therefore, solution conductivity in a solution of NaCl, is proportional to its concentration as described in **Equation 2.1** below (a and b are coefficients). Conductivity (σ) is the conductance in unit path length (**Equation 2.2**), In our system, we measure conductance (G) of solution in fixed path length (L) to show the ion concentration change in our CDI system (**Equation 2.3**). The unit of conductance is Siemens (S).

$$\sigma = a[\mathrm{Na}+] + \mathrm{b}[\mathrm{Cl}-] \quad \textbf{2.1}$$

$$\sigma = \frac{G}{L} \quad \textbf{2.2}$$

$$G = L(a[Na+] + b[Cl-]) \quad \textbf{2.3}$$

Conductivity meter is a common tool for solution conductivity measurement. Most conductivity meters use 4-ring conductivity probe with a built-in temperature sensor. (**Figure 2.1A**) Alternating current is applied on outer rings and voltage is measured on inner rings to give conductivity data. The conductivity probe is covered by an outer sheath to ensure the volume of sample solution stays constant.

We have tested the conductivity of NaCl solution of different concentration (0.03, 0.3, 3, 30 g/L) with HANNA HI4321 conductivity meter to prove proportionality of measured conductivity and NaCl concentration. (**Figure 2.1B**) The conductivity measured are in the unit of uS/cm.

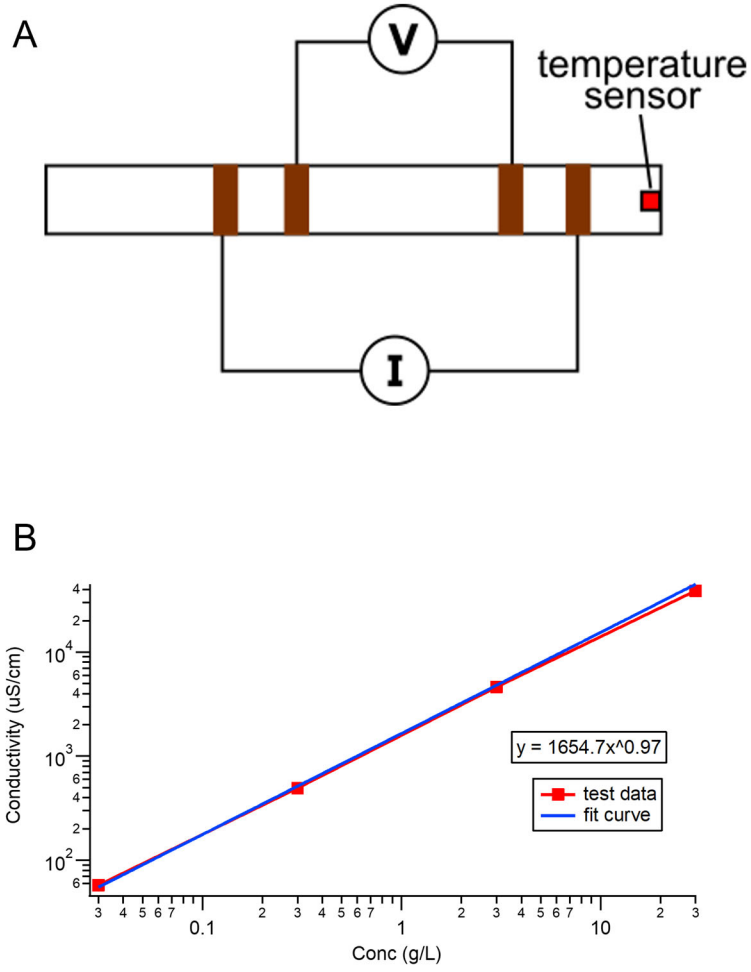

Figure 2.1 **A) Model of a 4-ring conductivity probe used in commercial conductivity meter B) Calibration curve from conductivity test of 0.03, 0.3, 3, 30 g/L NaCl solution with HANNA HI4321 conductivity meter.**

Conductivity (σ) is the conductance in unit path length (**Equation 2.2**). In our system, we measure conductance (G) of solution in fixed path length (L) to show the ion concentration change in our CDI system (**Equation 2.3**).

2.1.2. Instrument

An AC source for our solution conductivity measurement and a DC source for capacitive deionization are required to build a CDI cell and measure salt concentration. An arbitrary function generator (AFG) is a device that generates programmable electrical signal. Our system employs two AFGs with the Tektronix AFG1022C [80] providing an AC signal while the Tektronix AFG3022C [81] was the DC signal source.

In order to build in-situ CDI performance measurement system, we need to measure conductivity of NaCl solution in an electric field during desalination. The challenge is how to measure small AC signal in noisy environment. Lock-in amplifiers are pieces of equipment that detect signals at a single frequency, filtering noise and other unwanted signals at all other frequencies. The SR810 Lock-in amplifier [82] was used to read AC signal from our solution conductivity measurement.

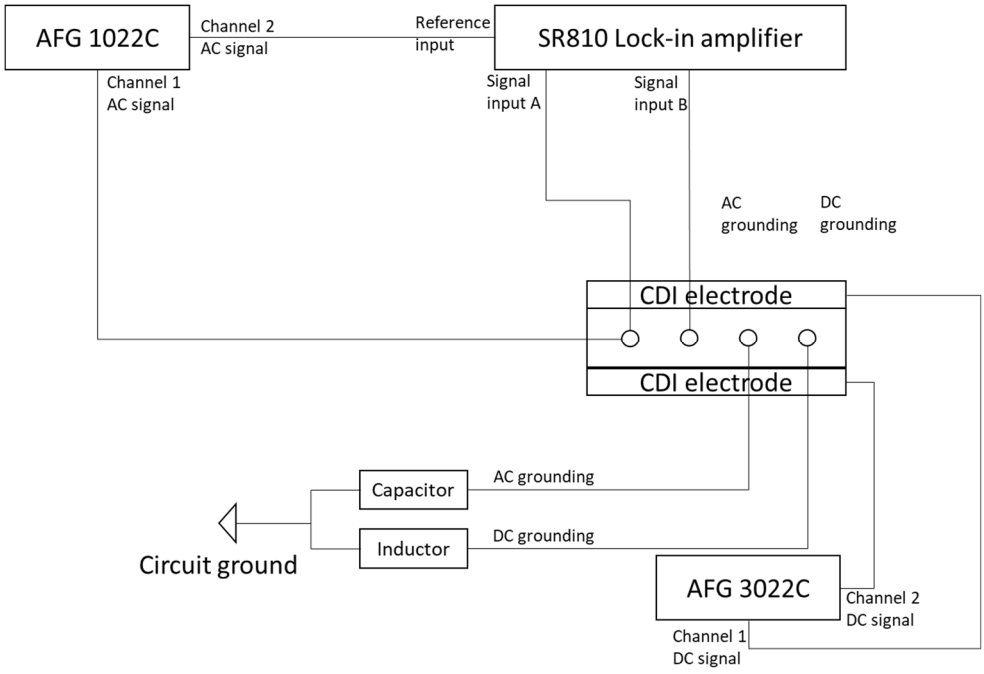

Figure 2.2 Schematic diagram of instrument connection

Figure 2.2 shows the connection of instrument in our experiment. The AFG1022C and the AFG3022C both have two independent channels. The AFG1022C outputs AC sine waves with same phase but different amplitude on its channels. The AFG1022C Channel 1 was connected to the solution conductivity measurement circuit while channel 2 was sent to SR810 reference input to provide frequency and phase reference. AC signal from solution conductance measurement was read by SR810 signal input A and B. The AFG3022C outputs a DC signal on CDI electrodes, channel 1 and channel 2 applies a different DC voltage on each CDI electrodes, with the DC voltage applied to each of CDI electrodes being adjustable. All devices used in this connection are earth grounded.

SR810 has two inputs: input A and input B. It reads AC voltage signal on both inputs. There are two modes of data output on lock-in amplifier: A and A-B. In A mode, lock-in amplifier outputs the voltage amplitude on A as data. In A-B mode, the lock-in amplifier subtracts the voltage reading at B from the reading at A, outputting the voltage amplitude of the resulting sine wave as data. We will use A-B mode to measure conductance of NaCl solution.

In order to measure charge input of our CDI system, we need to measure DC current across CDI electrodes. We used a transimpedance amplifier to convert DC current signal into voltage signal so that an analog device (NI-PCI-4461) installed on the computer can read and give DC current data.

2.1.3. Operational amplifier (op-amp) basics

Operational amplifiers (op-amps) are the backbone of analog electronics. Our setup uses custom circuitry, and as such, contains many op-amps. In order to describe the circuit in a manner accessible to future students, below is a short primer on these important devices. Operational amplifiers play an important role in electronics used for diagnostic and control of CDI systems. Because a typical AFG has very low power output, it cannot supply sufficient current for our experiments. As such, AFG signals need to be inputted into a power amplifier, which we have constructed using op-amp circuitry.

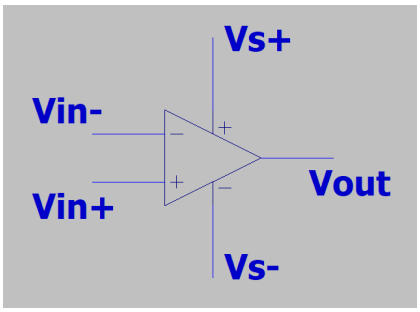

Figure 2.3 Circuit diagram symbol for an operational amplifier

As shown in **Figure 2.3**, an operational amplifier is a three-terminal device, with an additional two terminals Vs+ and Vs- providing power to the device from a DC power supply. The three terminals are the inverting input (V_{in-}), the non-inverting input (V_{in+}), and the output (V_{out}). Voltage supply (V_{s+} and V_{s-}) typically needs to be symmetric with respect to the circuit ground (for example +9V and -9V) to ensure correct operation of the op-amp.

In order to provide a clear view of how op-amps work, several basic rules of ideal op-amp need to be introduced:

(1) Ideal op-amps have infinite impedance at V_{in+} and V_{in-} to ensure no current flow into V_{in+} or V_{in-}.

(2) Op-amps work to maintain an equal voltage between inverting and non-inverting inputs (i.e., $V_{in-} = V_{in+}$) by adjusting V_{out} when there is a feedback loop from V_{out} to input terminals. (3)

(3) Open loop gain (A_{ol}) of an ideal op-amp is infinite in the ideal case. In other words, if we provide to the input terminals (V_{in-} and V_{in+}) different voltages, the op-amp would amplify the difference between V_{in+} and V_{in-} with open loop gain (A_{ol}), to cause an infinite large V_{out} (**Equation 2.4**) without a feedback circuitry.

$$V_{out} = A_{ol}(V_{in+} - V_{in-}) \qquad \textbf{2.4}$$

Therefore, to make op-amp work in designated way, feedback from V_{out} to V_{in+} or V_{in-} is almost always necessary.

In practice, the behavior of an op-amp deviates from ideal behavior in several ways. For example, the input impedance of op-amp is not infinite, but it tends to be

relatively large (~47k ohm), preventing most, but not all current from flowing into inputs. As another example of non-ideal behavior, the open loop gain is limited by the supply voltage. Without any other limits, If the supply voltage is ±9V, the maximum V_{out} would be ±9V. Op-amps usually have a current limit as well, this limit is different for different op-amps and represents a key performance metric when selecting the correct op-amp for a given application.

2.1.4. Example op-amp circuits

A voltage follower, also known as unity gain op-amp, is an op-amp circuit often used for supplying voltage or isolating measurements from the rest of an experiment (**Figure 2.4**). When a voltage is applied at V_{in+}, the op-amp would adjust V_{out} to make $V_{in-} = V_{in+}$. Therefore, V_{out} would be the same voltage as V_{in+} hence providing unity gain. An additional feature of this simple circuit is that the power output of the op-amp is limited by properties of the op-amp and not of the signal source. It is therefore often useful as a simple power amplifier for devices like AFGs which are very limited in their power output.

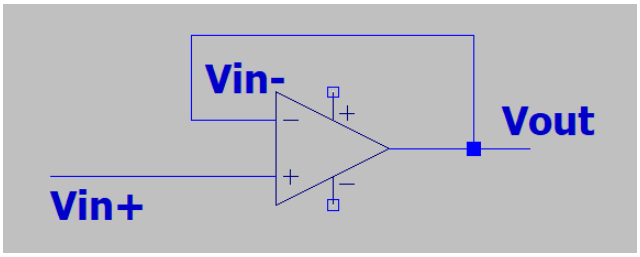

Figure 2.4 Circuit diagram of a voltage follower

A current follower is an op-amp circuit often used for amplifying voltage or supplying current. The structure of current follower op-amp is shown in **Figure 2.5**. V_{source} is the constant voltage from voltage source, R1 and R2 are resistors, GND represents circuit ground.

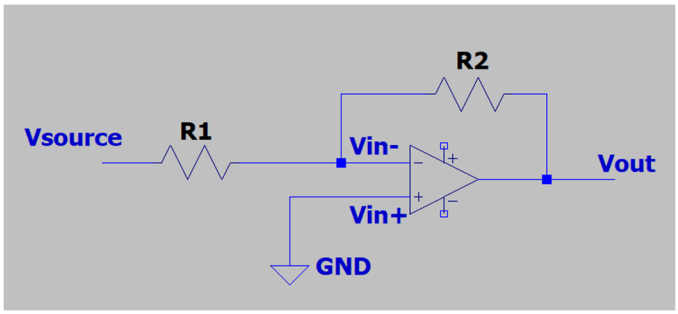

Figure 2.5 Circuit diagram of a current follower

In this circuit, V_{in-} is a virtual ground as it has 0 V potential but not direct connected to the circuit ground. This is because of op-amp always outputting a V_{out} that keeps V_{in-} = V_{in+}. when V_{in+} = 0 V, V_{in-} would also be kept at 0 V.

Current follower op-amp would output a negative voltage to maintain current through known resistor R2 to equalize the current flowing through R1. As the equation shown below, this makes V_{out} proportional to the current through the solution. By measuring V_{out} we would know current (I) through R1 (**Equation 2.5**).

$$I = \frac{V_{source}}{R1} = -\frac{V_{out}}{R2} \qquad \textbf{2.5}$$

2.1.5. Voltage source

Voltage source is a device which outputs constant voltage independent of load resistance. AFG1022C channel 1 amplified by a unity gain amplifier is a voltage source. To measure solution conductance with a voltage source, we apply a constant voltage (V) across the solution and measure the current (I). The conductance of solution is proportional to the current we measured as **Equation 2.6** shows.

$$G = \frac{1}{R} = \frac{I}{V} \qquad \textbf{2.6}$$

Based on the current follower op-amp circuit, we made some changes to make this part more stable in our experiment. (**Figure 2.6**) Firstly, op-amp output was connected to the virtual ground and actual ground through resistors with same resistance R to improve

V_{out} signal stability. Secondly, a capacitor with large capacitance was added before virtual ground to filter DC current during CDI electrodes charging. The capacitance of this capacitor should be large to minimize the capacitive impedance influence on the current (I) through solution (Rs).

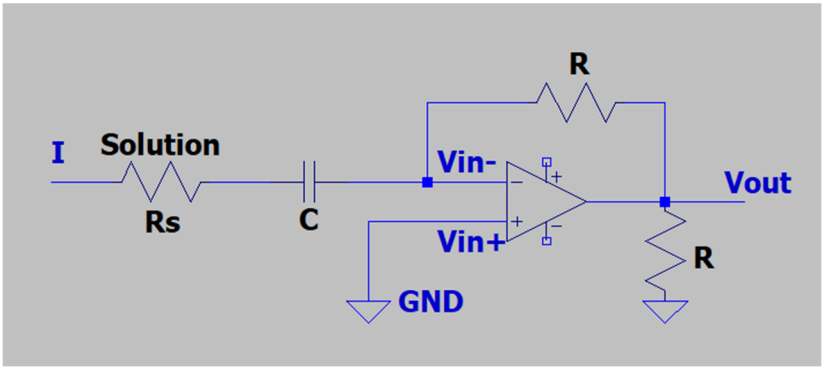

Figure 2.6 Current follower op-amp circuit optimized for our experiment

The first-generation solution conductance measurement system employed a constant voltage source. Between two CDI electrodes we have 3 wires inside the cell: V_{out}, A, and B (**Figure 2.7B**). Constant AC voltage from AFG1022C was amplified by a unity gain op-amp and sent to the wire in the cell labeled Vout. The current passing through the solution from Vout to A and B wires. Because the distance of solution from Vout to wire A is different from Vout to wire B. Current that flows through wire A is different from that through wire B. A current follower was connected to A and B wires in the cell to transfer current signal into proportional voltage signal so that current on wire A and wire B can be separately read by lock-in amplifier (**Figure 2.7A**). Lock-in reads voltage signal at input A and input B, outputs voltage difference between input A and B as V_{A-B}, which is proportion to the current difference between wire A and wire B. It is observed that V_{A-B} increases as solution concentration increases. The rationale of using two wires to detect current is that any parasitic currents emanating from DC voltage applied on CDI electrodes would be equal in both wires and would therefore be cancelled upon taking their difference. However, this configuration suffers from DC leakage current emanating from the CDI electrodes that did not cancel out. This primarily occurred shortly after the DC voltage was changed, this sharp change in voltage introduces a noise signal as required by the Fourier transform of a step function. As a result, a high pass filter was added between current follower and lock-in amplifier to eliminate the noise signal of voltage at beginning and end of CDI electrodes charging process.

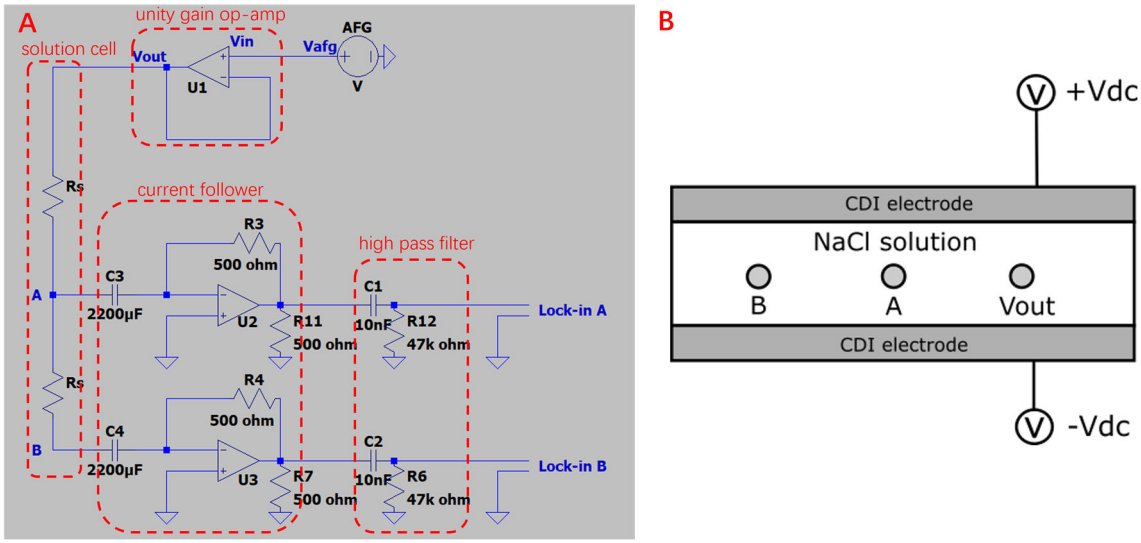

Figure 2.7 **(A) Voltage source solution concentration measurement circuit diagram (B) Profile of our previous CDI cell with voltage source conductance measurement circuit (Vout, A, B are titanium wires)**

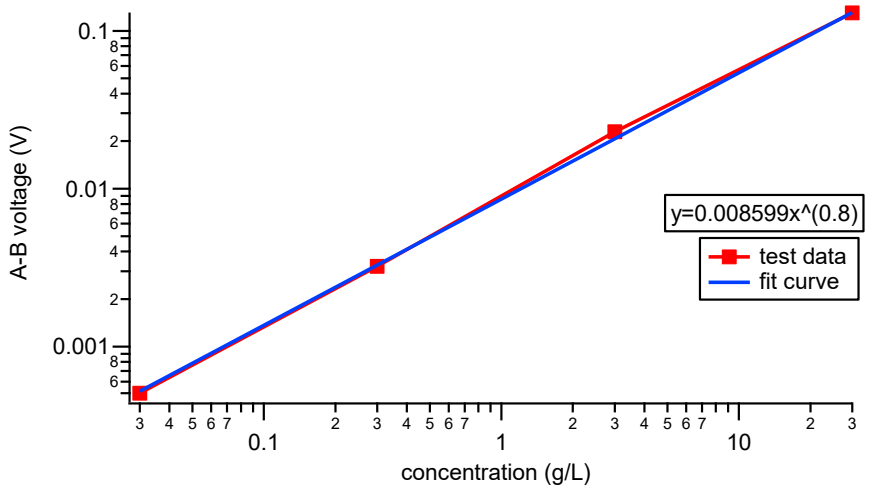

Figure 2.8 **Calibration curve obtained from cencentration test for NaCl standard solutions (0.03, 0.3, 3, 30 g/L) with voltage source circuit**

Conductance measurement on NaCl standard solutions (0.03, 0.3, 3, 30 g/L) has been done and a calibration curve of V_{A-B} vs concentration (**Figure 2.8**) has been fitted. The calibration curve is a power law with the exponent equal to 0.8, which is encouraging, but not close enough to the theoretically expected linear relationship as **Equation 2.1** shows. The non-linearity relationship between V_{A-B} and concentration indicates measurements in higher concentrations are not accurate enough to reveal solution concentration from the V_{A-B} reading.

We hypothesized that the non-linearity of calibration curve in the voltage-source/current measure solution conductivity experiment was a result of electrolyte-electrode interface impedance (R_i) between wires and the solution. Electrolyte-electrode interface impedance results from the electric double layer around the wire surface, electrochemical reactions happening on the electrode, the formation of a native oxide around the wire electrodes, or the diffusion of electrolyte ions around the electrode[83]. As shown in **Equation 2.7**, considering interface impedance, current across the solution is not only determined by the solution resistance (Rs), but also depend on this unknown interface impedance (R_i). This interface impedance is less related to the solution concentration but more related to the surface area of wires. In high concentration NaCl solution, R_s is small, making the effect from R_i more obvious. This causes the phenomenon that relationship between $V_{A\text{-}B}$ and concentration have more deviation from linearity when concentration is higher, which eventually results in a power law curve like fitting. It is anticipated that when salt concentration is significantly higher than 30 g/L, which results in nearly zero Rs, the A-B voltage would deviate from the power law curve fit and nearly reach a plateau.

$$I = \frac{V_{source}}{Rs + R_i} \qquad \textbf{2.7}$$

2.1.6. Current source

Due to the fact that the existence of electrolyte electrode interface impedance severely influences voltage source system's accuracy of conductance measurement in concentrated solutions, we decided to use a current source to measure solution conductance in the most advanced generation of solution conductivity meter employed in this thesis.

A current source is a device that ideally outputs a constant current independent of the load resistance in the circuit. According to Ohm's law, as current (I) across the circuit is constant, larger load resistance (R_{load}) would cause a larger voltage output (V_{out}) from

current source. In this case, conductance (G) is proportional to the reciprocal of voltage (**Equation 2.8**).

$$G = \frac{1}{R_{load}} = \frac{I}{V_{out}} \tag{2.8}$$

A Howland current source is the configuration we used for building our solution conductivity test system (**Figure 2.9**). There are four fixed resistors (R1, R2, R3, R4) and a high frequency op-amp (LM7171) in this configuration.

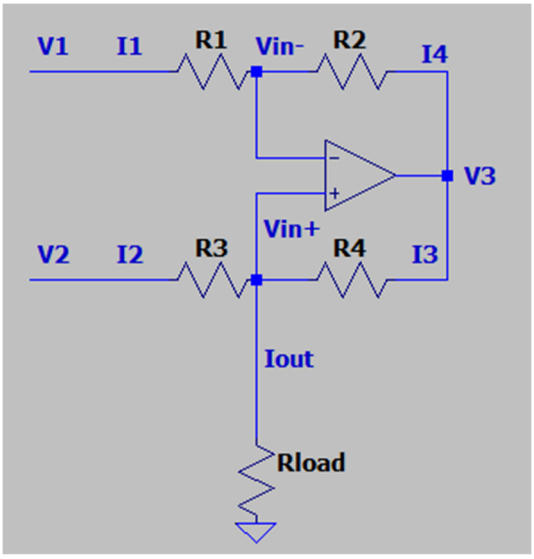

Figure 2.9 Configuration of Howland current source

According to the basic law of ideal op-amp working, there is no current flowing into either input of op-amp. Therefore, when there is a voltage difference between V1 and V2, the following equations can be derived.

$$I_1 = I_4 = \frac{V_{in-} - V_1}{R_1} = \frac{V_3 - V_{in-}}{R_2} = \frac{V_3 - V_1}{R_1 + R_2} \tag{2.9}$$

$$I_2 = \frac{V_2 - V_{in+}}{R_3} \tag{2.10}$$

$$I_3 = \frac{V_3 - V_{in+}}{R_4} \tag{2.11}$$

$$I_{out} = I_2 + I_3 \quad \textbf{2.12}$$

Because $V_{in+} = V_{in-}$, $V_3 - V_{in+} = V_3 - V_{in-}$, **Equation 2.13** can derived by combining **Equation 2.10** and **Equation 2.11**

$$I_3 = \frac{I_1 R_2}{R_4} \quad \textbf{2.13}$$

Transforming from **Equation 2.9**, $V_{in-} = I_1R_1+V_1$. Emerging this into **Equation 2.10** we can get **Equation 2.14**.

$$I_2 = \frac{V_2 - (I_1 R_1 + V_1)}{R_3} \quad \textbf{2.14}$$

Because $I_{out} = I_2 + I_3$, Equation 2.13 and Equation 2.14 has expressed I_3 and I_2, we can get **Equation 2.15**

$$I_{out} = \frac{V_2 - (I_1 R_1 + V_1)}{R_3} + \frac{I_1 R_2}{R_4} = \frac{V_2 - V_1}{R_3} + I_1(\frac{R_2}{R_4} - \frac{R_1}{R_3}) \quad \textbf{2.15}$$

In the application of the configuration, the ratio of $R_2 : R_4$ is always controlled to be equal to the ratio of $R_1 : R_3$, so that I_{out} would be proportion to voltage difference between V_2 and V_1. While V_1 is normally connected to the ground, which made I_{out} only depends on V_2 (**Equation 2.16**)

This configuration allows us to control the output current by changing applied voltage (V_{in}) on AFG1022C. V_{in+} is proportional to the resistance of load (R_{load}) in order to supply constant current (**Equation 2.17**), which allows solution conductance measurement via reading voltage of V_{in+}.

$$I_{out} = \frac{V_2}{R_3} \quad \textbf{2.16}$$

$$V_{in+} = I_{out} R_{load} \quad \textbf{2.17}$$

2.1.7. Final CDI test instrumentation

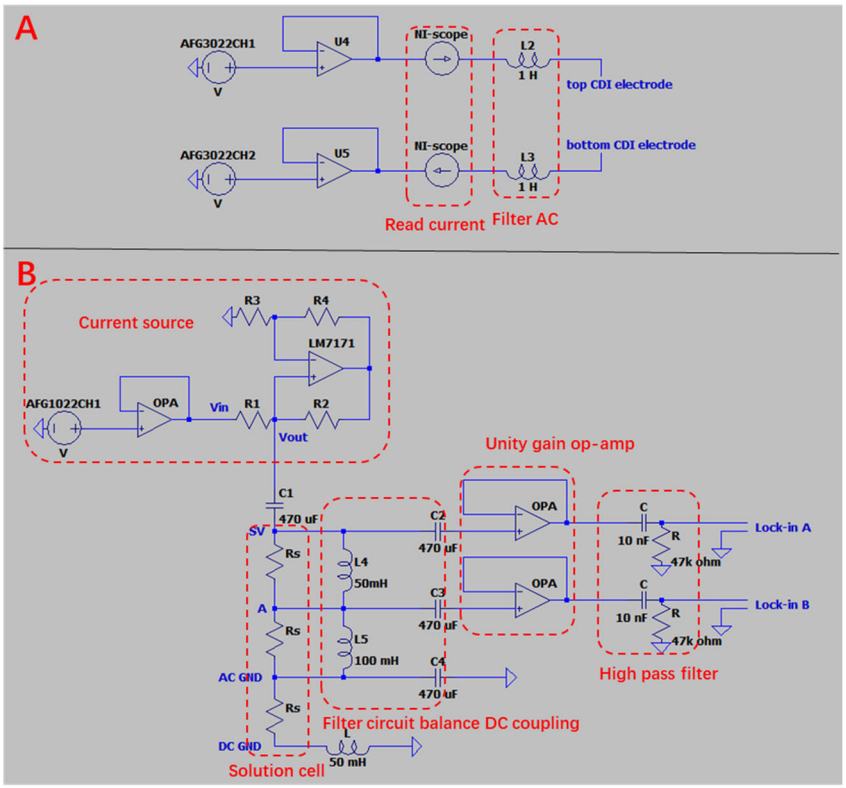

Figure 2.10 (A) CDI cell DC charging circuit (B) Solution concentration measurement circuit

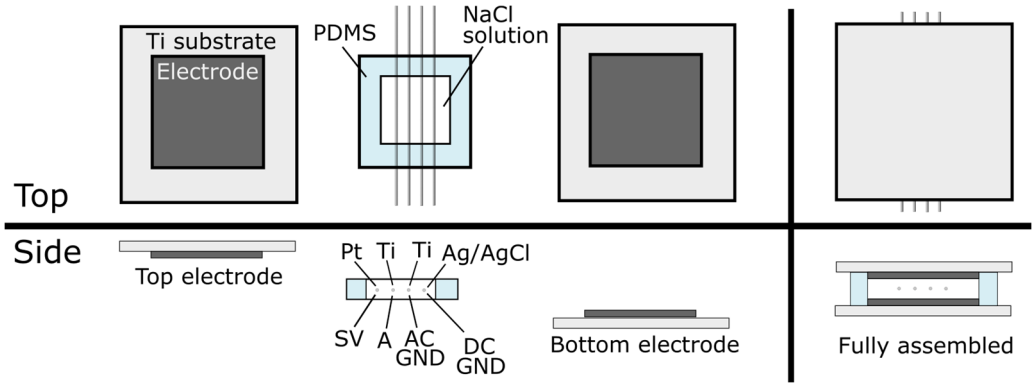

Figure 2.11 Detailed top and side view of our CDI cell (SV, A, ACGND, DCGND are consistent with circuit diagram in Figure 2.9)

Eventually, we built a current source solution concentration measurement system in the middle of our CDI cell.

Figure 2.10A is the circuit diagram for CDI system. Constant DC voltage from AFG3022C was amplified by unity gain op-amps and was applied on top and bottom CDI electrode separately. DC current was converted to a voltage via a transimpedance amplifier constructed by the SFU electronics shop. This volage was continuously read by an analog to digital converter (NI-scope) installed into the PC that controlled the experiment. The inductors L2 and L3 prevents DC signal from impacting the AC measurement of solution concentration.

Figure 2.10B is the solution concentration measurement circuit. The current source supplies constant amplitude of AC current through the solution from SV to the AC GND. The frequency of AC current is 100kHz. Voltage difference between SV and A was read by lock-in amplifier. Unity gain op-amps was connected to SV and A to decouple lock-in amplifier from current source load, so that lock-in amplifier voltage measurements would not affect current source voltage output. High pass filters were added to filter noise signal from sudden DC voltage change. During CDI cell charging, capacitors C1, C2, C3, C4 minimized DC coupling from CDI electrodes, while inductors L4 and L5 balanced the rest DC coupling on wire SV, A, AC-GND. C1 and C4 need to have high capacitance to minimize capacitive impedance at the moderate frequencies used. DC-GND determines reference voltage for DC voltage applied on CDI electrodes, 50 mH inductor L was connected to DC-GND to prevent AC current from affecting this electrode.

Figure 2.11 shows the top and side view of our CDI cell. We use 1'×1' titanium sheet as our substrate, the CDI electrode material was fabricated on the substrate. CDI electrodes at top and bottom were sandwiched a ring made by crosslinked polydimethylsiloxane (PDMS). Four metal wires in the middle of PDMS ring participate in solution concentration measurement corresponding to SV, A, AC-GND, and DC-GND in **Figure 2.10B**. We choose platinum for SV to prevent corrosion caused by possible high voltage. We use AgCl wire for our DCGND as a stable reference potential. NaCl solution was injected into CDI cell by syringe on one side. During injection, old solution would be pushed into another syringe on the opposite side of cell.

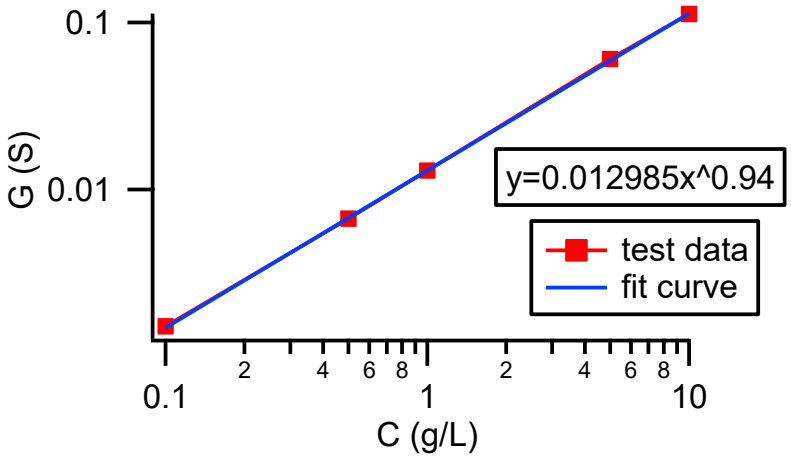

Figure 2.12 Calibration curve obtained from concentration test for NaCl standard solutions (0.1, 0.5, 1, 5, 10 g/L) with current source circuit

We obtained a calibration curve of conductance vs NaCl concentration with this CDI performance measurement setup (**Figure 2.12**). The calibration curve has a power law much closer to demonstrating its utility as a conductance and therefore concentration meter.

2.2. Activated carbon electrode fabrication

In order to test our cell and provide a comparison to a standard CDI material we fabraicated activated carbon electrodes onto our titanium current collectors. Activated carbon electrodes are fabricated following the procedure of Hou et.al[41]. Activated carbon powder (US mesh 40) was mixed with polyvinylidene fluoride (PVDF) polymer (M.W=534,000, Sigma Aldrich) binder in N,N-Dimethylacetamide (DMAc) solution to make carbon slurry. PVDF content was 15 wt.% of activated carbon. Slurry concentration was controlled at 25 g/L. Carbon slurry was drop casted on titanium substrate and dried under 120 ℃ for 2 hr to form carbon electrode that was well-adhered to the substrate. Then, carbon electrode was further dried in an 80 ℃ vacuum oven for 2 hr to ensure all organic solvents are removed.

2.3. PEDOT: PSS electrode fabrication

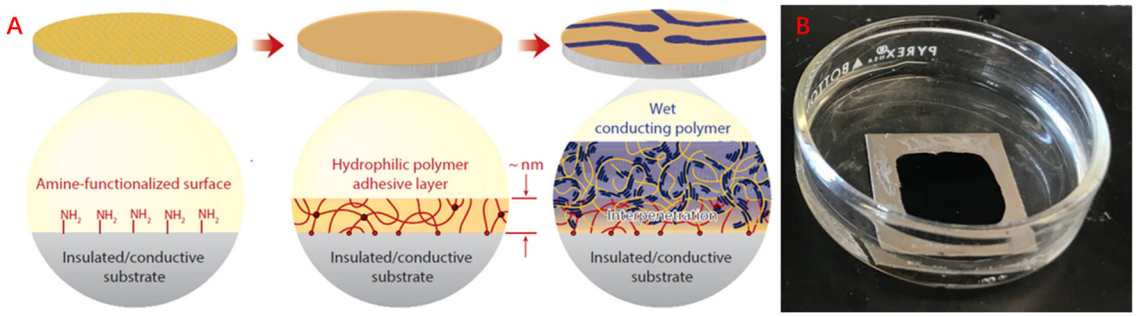

Figure 2.13 (A) Polyurethane chemistry applied to improve PEDOT:PSS adhesion on substrate (B) picture of our PEDOT:PSS film on titanium substrate

In order to test PEDOT:PSS as an electrode material for CDI, very thick films are required. Unfortunately, thick films also have a pronounced tendency to delaminate from the titanium current collectors when they swell in water and when filled with ions during device operation. Inspired by Inoue et.al [84], we use polyurethane (PU) as a binder to increase our PEDOT:PSS film adhesion on titanium substrate. (**Figure 2.13**) Amine functionalized surface would make better connection with PU, while PEDOT:PSS dispersion can permeate and combine with PU layer to have better adhesion on surface.

Silane solution was prepared by dissolving 1 w/v.% 3-aminopropyltriethoxysilane (3-ATES) in 100 mL deionized water then add 10 μL of glacial acetic acid. PU solution was prepared by dissolving 3 wt.% polyurethane (HydroMed D3, AdvanSource Biomaterial) in mixture of ethanol and 5 v/v.% deionized water.

PEDOT:PSS dispersion was prepared by dissolving dry PEDOT:PSS pellets in a mixture of propylene glycol and 0.3 g/L NaCl solution (30:70 = propylene glycol: NaCl solution), 2 wt.% of 3-glycidoxypropyltrimethoxysilane (GOPS) was added as crosslinker for PEDOT:PSS. PEDOT:PSS concentration of the dispersion was controlled at 5 g/L. The reason for having NaCl solution in our PEDOT:PSS dispersion is to give space in PEDOT:PSS film to allow salt adsorption, this helped dramatically to eliminate PEDOT:PSS delamination during the CDI charging process.

Titanium substrates were cleaned by soaking in 15% HCl for 1 hr at 60 ℃. Then the cleaned titanium was soaked in prepared silane solution for 1 hr at room temperature to form amine self-assembled monolayer. PU solution was then spin coated on the amine

functionalized titanium surface at 1000 rpm for 30 s. After spin coating, PU coated substrate was annealed under 90 ℃ for 1 hr.

PEDOT:PSS was drop casted on the annealed PU coated titanium substrate and air dried overnight at room temperature. This allows PEDOT:PSS to have sufficient time to permeate PU layer and interact with PU polymer chain. Air dried PEDOT:PSS was then annealed for 1 hr at 120 ℃ to make PEDOT:PSS film

Surface treatment steps are necessary for optimizing CDI performance of PEDOT:PSS film. PEDOT:PSS film was soaked in 0.1 mM polyethyleneimine (PEI) (Mn~10000) solution at RT for 1 hr, then soaked in 1 M H_2SO_4 at RT for overnight in order to remove the NaCl introduced in the procedure and improve the conductivity of the film.[85]

To prepare the anion conducting electrode, an additional treatment step was required. Samples were immersed in 0.1 M $CaCl_2$ solution to replace the Na^+ typically present in PEDOT:PSS films with Ca^{2+}. Calcium was chosen because of its 2+ charge, the non-toxic nature of calcium, and the low solubility of $CaSO_4$ in water. Presumably, the last factor makes Ca^{2+} transport in PEDOT:PSS significantly slower than Cl^- allowing it to be incorporated in order to maintain charge balance of the solution. Positive potentials were not applied to the anion collecting electrode, as it tended to degrade electrode performance over time.

2.4. CDI Electrodes conditioning

2.4.1. Activated carbon

After compacting CDI cell, MilliQ water [2] was first injected into the CDI cell to wet the carbon electrodes, then 0.5 g/L NaCl solution was injected. After injection of NaCl solution, we charged the CDI cell with top voltage 0.6 V and bottom voltage -0.6 V for 20 min (Ag/AgCl as ground). A curve like **Figure 2.14** is typically observed during the charging, electrode charging starts at 10 s and ends at 1200 s. As DC voltage was applied on the top and bottom electrodes, conductance of solution falls because of capacitive deionization. After the first plateau, conductance starts to increase a bit due to the expulsion of co-ions. After charging stops, electrodes will discharge, and solution

[2] MilliQ water: ultrapure water produced by Milli-Q™ direct water purification system

conductance will firstly increase a little, then continue to decrease. We call this step the electrode preparing process. This process helps the wetting of the dry activated carbon electrode and improves electrode stabilization for further tests.

After the electrode preparing process, we need to wash the electrodes by injecting milli Q water into the cell. The CDI cell need to be charged with top voltage 0.6 V and bottom voltage -0.6 V in milliQ water for 20 min or longer. During charging, solution conductance increase can be observed, indicating adsorbed salt coming out from electrodes. MilliQ water was constantly injected to wash away the expelled ions until solution conductance was stabled at limit of detection (stay below 1e-4 S for 100 seconds). After charging ends, the CDI electrodes need to be discharged until current observed from discharging is below 2e-5 A. This is called washing process. The washing process is also needed before changing concentration of feed solution. The washing process expels the co-ions that are attracted to the porous electrode surface by the adsorbed counter-ions when applied voltage stopped.

After washing process, carbon electrodes are ready for desalination The first desalination cycle should charge with 0.6V on positive electrode and -0.6V on negative electrode. The first cycle should be longer than intended experiment charging time. We take second desalination cycle as our experimental data since the first cycle is for CDI system to achieve equilibrium in chosen concentration of feed water.

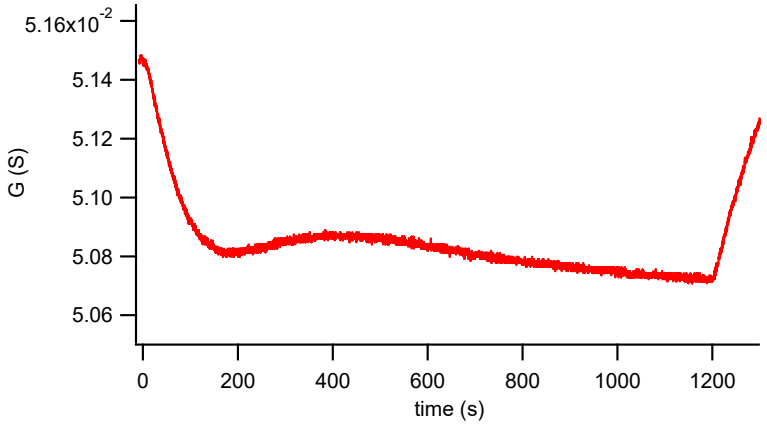

Figure 2.14 Solution conductance change in 5 g/L NaCl solution during 20 min conditioning charging of CDI cell with activated carbon electrodes

2.4.2. PEDOT:PSS

Before experiment, PEDOT:PSS electrodes are soaked in 1 g/L NaCl solution without any voltage applied. An increase of solution conductance is typically observed in this process (**Figure 2.15**). The soaking process took an hour for solution conductance to stop increasing. Soaking process is needed only the first time PEDOT:PSS electrodes compacted into CDI cell. Soaking process stabilizes the dry PEDOT:PSS electrodes in an aqueous electrolyte solution.

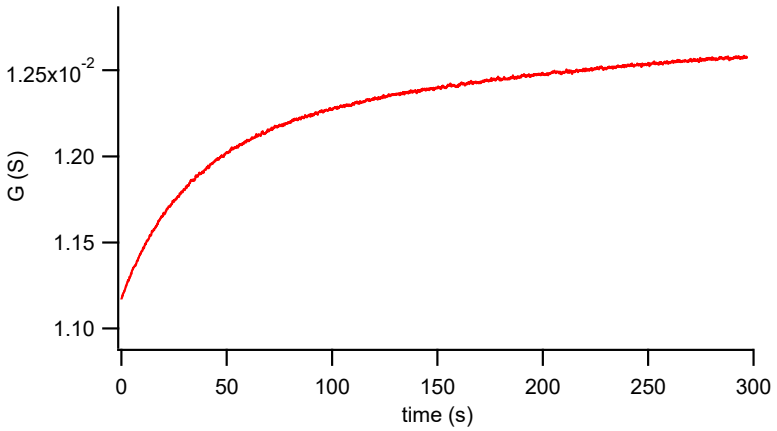

Figure 2.15 Solution conductance increase during soaking PEDOT:PSS electrodes in 1 g/L NaCl solution

Once solution conductance stabilized in the soaking process, MilliQ water is injected into the CDI cell. Then we applied 0 V on positive electrode and 1.2 V on negative electrode for 20 min or longer to release ions in electrodes, solution conductance increase was observed during voltage applied. MilliQ water was constantly injected to wash away the expelled ions until solution conductance was stabled at limit of detection (stay below 1e-4 S for 100 seconds), then electrodes were discharged under 0 V applied on both electrodes until current from discharging decrease under 2e-5 A. We called this step reverse charge process. Reverse charging process is also needed before we change concentration of feed solution. Reverse charge process expels NaCl ions trapped in PEDOT:PSS electrodes out of the electrodes, promises accurate CDI performance measurements.

After soaking process and reverse charge process, NaCl solution is injected into the system for desalination. In the first cycle, we applied 0 V on positive electrode and -1.2 V on negative electrode. In low concentrations from 0.1 g/L to 1 g/L, solution

conductance will firstly decrease, then increase to a certain point, then decrease again during the first cycle. We stop the applied voltage when we saw solution conductance stopped to increase or when first cycle time exceeds four times of our intended experiment charging time. In high concentration like 5 g/L and 10 g/L, solution conductance would keep decreasing during the first cycle. We stop when first cycle time exceeds our intended charging time for the experiment. After the first cycle, we would wait until the cell completely discharged to run second cycle. When discharging current in the cell drop below 2e-5A, we can say it is completely discharged. The first cycle is for system to achieve equilibrium in chosen concentration of feed water. We took second cycle of desalination as our experimental data.

We are measuring CDI performance in same concentration with different applied voltage, as well as in different concentrations with same applied voltage. For MSAC tests for both material, first run only lasts 300 seconds, while the second run would be more than 20 minutes to obtain MSAC of the material.

Chapter 3.
Results and Discussion

This section provides details regarding the result from desalination performance test for activated carbon and PEDOT:PSS. The effect of applied potential and feed water concentration on SAC and CE during 300 s desalination was studied in this experiment. The MSAC of both materials in different feed water concentration have also been reported and discussed.

In the experiment studying the affect of applied potential on desalination behaviour, saltwater concentration was controlled at 0.5 g/L, while applied voltage difference between two CDI electrode was varied (0.4 V, 0.6 V, 0.8 V, 1.0 V, and 1.2 V). In the experiment studying the feed water concentration on desalination behaviour, applied voltage difference between two CDI electrodes was controlled at 1.0 V, while 5 feed water concentrations were used for desalination test (0.1 g/L, 0.5 g/L, 1 g/L, 5 g/L, and 10 g/L).

In the experiment studying MSAC, applied voltage difference between two CDI electrode was kept at 1.0 V, while 4 concentrations of feed water were used for desalination test. The CDI electrode charging process was over 20 minutes or longer until solution conductance barely change with time.

The applied voltage on CDI electrodes during charging was different for activated carbon and PEDOT:PSS. In activated carbon CDI cell, electrodes were symmetrically charged, which can be interpreted as when there is a voltage difference of 1.0 V, 0.5 V was on positive electrode while -0.5 V on negative electrode. In PEDOT:PSS cell, electrodes were asymmetrically charged. Positive electrode of PEDOT:PSS cell was always kept 0 V, while negative electrodes have -1.0 V at voltage difference of 1.0 V. All voltages above are refer to Ag/AgCl reference electrode.

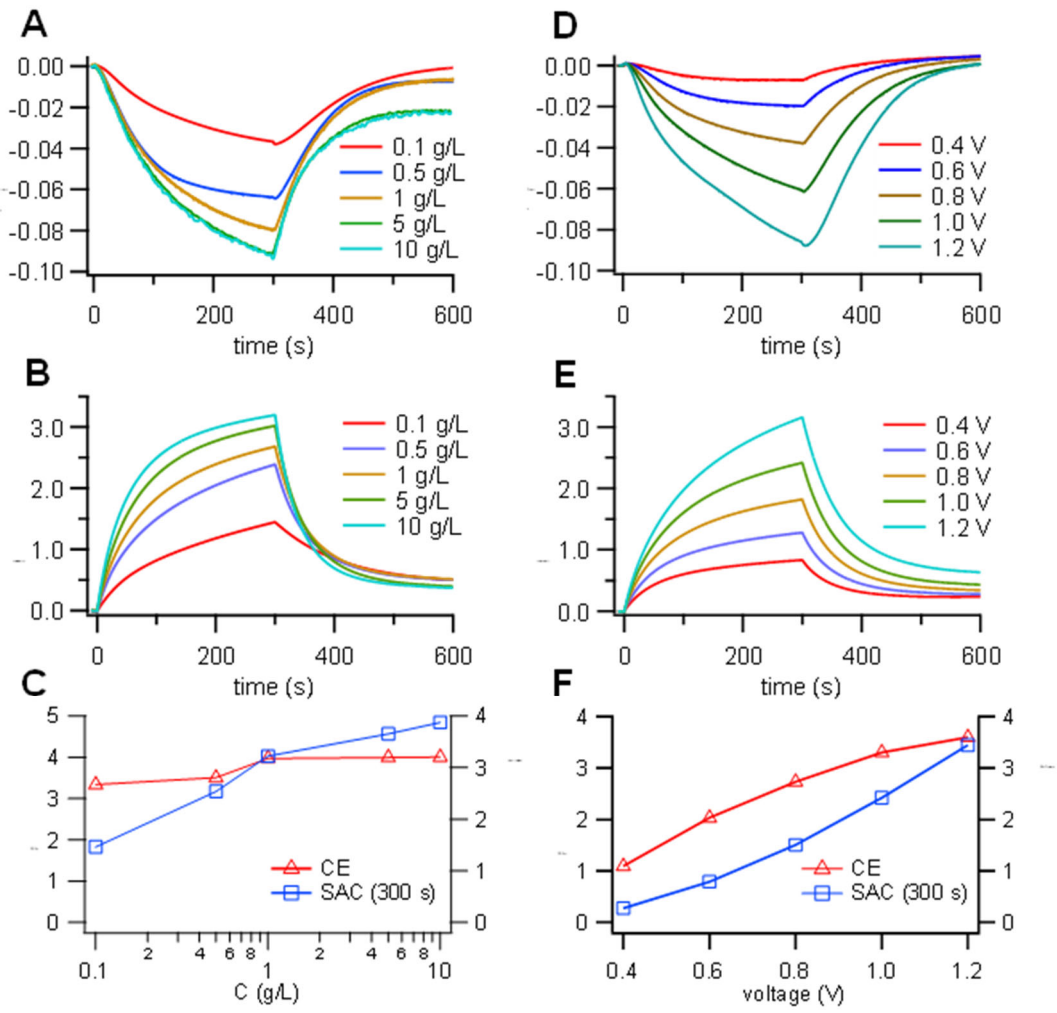

Figure 3.1. Activated carbon CDI cell 300 second desalination test (A) Solution concentration change (B) integrated current (C) CE and SAC vs feed water concentration; (D) Solution concentration change (E) integrated current (F) CE and SAC vs applied voltage

Figure 3.1 shows the response observed during the charging and discharging of activated carbon electrodes in contact with a solution of NaCl. **Figure 3.1A** shows the change in solution concentration as a function of time for several concentrations. At t=0 seconds, a voltage of 0.5 V is applied to one electrode, while a voltage of -0.5 V is applied to the other. The concentration decreases until the potential is removed at t=300 seconds, allowing ions re-enter the solution. **Figure 3.1B** shows the integrated current flowing to the current collectors as a function of time for several concentrations. As expected, the curves resemble the inverse of the desalination behavior. **Figure 3.1C** shows the salt adsorption capacity (SAC = mg NaCl removed per g of electrode material) as a function

of concentration. The SAC increases logarithmically with the concentration of the solution as a result of the slight increase in double layer capacitance. The values obtained are consistent with previous reports [86], and typical for activated carbon electrodes that have not been scrupulously optimized. **Figure 3.1C** also displays the charge efficiency (CE = mol NaCl removed per mol of electrons flowing to the electrodes, here plotted at t=300 s) as a function of concentration. The CE is approximately flat across the concentration range and reflects a concentration independent leakage current flowing from the desalinating electrodes into the solution.

The voltage dependence of the desalination behavior of activated carbon electrodes is shown in **Figure 3.1D-F** with the potential applied symmetrically to the current collecting electrodes. In these experiments, the solution concentration was 0.5 g/L. As above, salt is removed from solution upon the application of a potential, and returned to the solution upon removal of the potential. Agreement with the measured charge flowing to the current collecting electrodes demonstrates that the desalination behavior is electrically modulated and is not simply passive adsorption. **Figure 3.1F** displays SAC at t=300 s as a function of voltage which increases with applied potential. A simple RC circuit model would predict a purely linear increase however, we observe a slight nonlinearity as a result of the potential dependence of the electrostatic double layer capacitance. As a result of the increase in SAC, the CE increases with applied potential, saturating at the largest potentials presumably as a result of increasing leakage current.

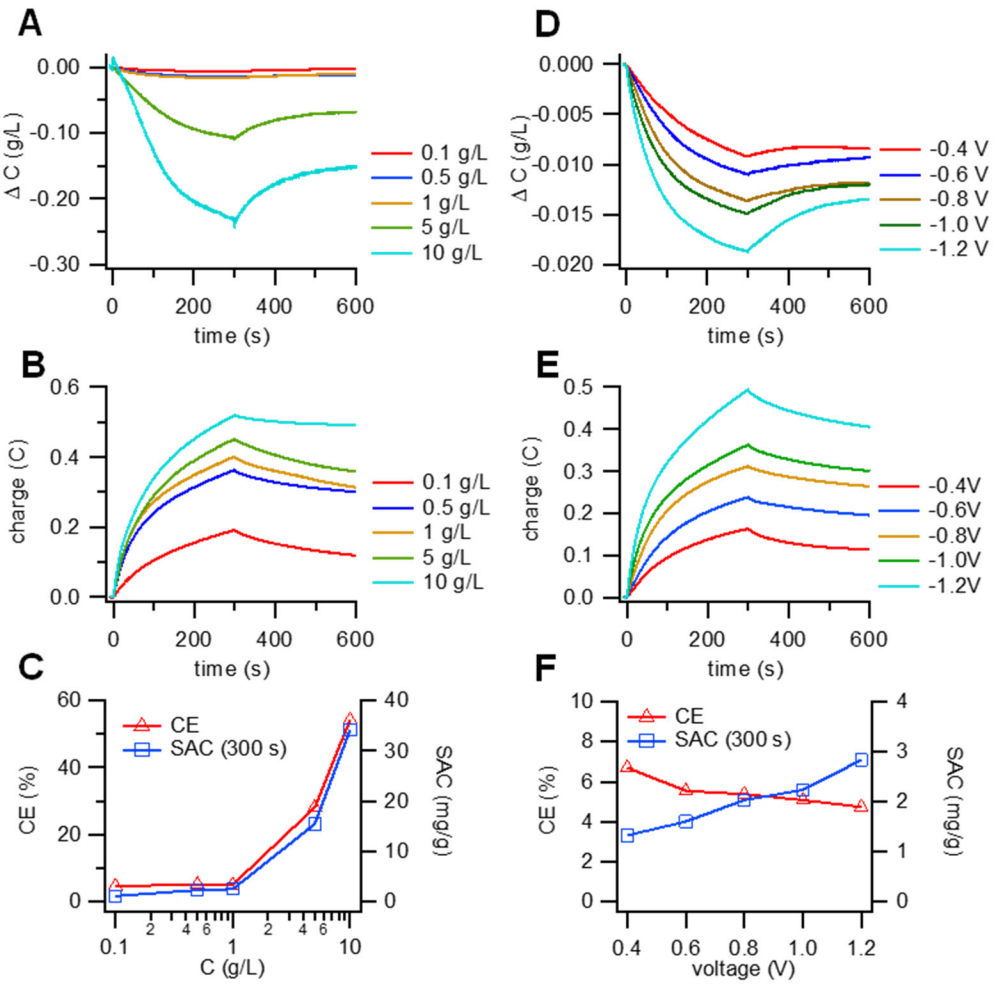

Figure 3.2 **PEDOT:PSS CDI cell 300 second desalination test (A) Solution concentration change (B) integrated current (C) CE and SAC vs feed water concentration; (D) Solution concentration change (E) integrated current (F) CE and SAC vs applied voltage**

The capacitive deionization behavior of PEDOT:PSS electrodes is demonstrated in **Figure 3.2** with the decrease in salt concentration as a result of applied potential being shown in **Figure 3.2A**. The salt concentration decreases as potential is applied, recovering slowly when the potential is removed. **Figure 3.2B** shows the integrated current passed to the charge collecting electrodes as a function of time. The collected charge grows after the potential is applied and is returned to the circuit when potential is removed. However, the magnitude of the integrated charge at low concentrations is significantly higher than the salt removed from solution. We interpret this as reflecting a much larger leakage current emanating from the PEDOT:PSS electrode than is observed with activated carbon. This is more clearly visualized from the CE at t=300 s plotted in **Figure 3.2C**. The CE at

low concentrations is very low, following the SAC as concentration increases. This behavior is consistent with a concentration independent leakage current; as more salt is removed from solution, the contribution to the current resulting from deionization behavior becomes a larger percentage of the overall current. The SAC at t=300 s increases dramatically with concentration, which is totally different from activated carbon. This indicates the desalination behavior of PEDOT:PSS is mechanistically different than the electric double layer processes associated with activated carbon.

The voltage dependence of the deionization behavior of PEDOT:PSS is shown in **Figure 3.2D-F** for a concentration of 0.5 g/L. The decrease in solution concentration as a function of time is clearly observed in **Figure 3.2D**, which is in good agreement with the integrated charge from the current collecting electrodes shown in **Figure 3.2E**. As with activated carbon, this demonstrates that observed deionization behavior is modulated by the voltage, rather than being due to passive adsorption. In **Figure 3.2F** the SAC at t=300 s is plotted as a function of applied potential. Consistent with the broad, flat density of electronic states in PEDOT:PSS, the amount of salt taken in by the electrode is linear with voltage. Over this potential range, the CE is observed to decrease with applied potential, indicative of an increasing leakage current flowing into the solution while potential increase, the magnitude of which can be qualitatively described in terms of a voltage independent resistance. Strategies for decreasing the magnitude of leakage currents in PEDOT:PSS capacitive deionization cells appears to be an important avenue of investigation for technological applications, especially when used with lower concentration feed streams.

It is observed from the concentration change vs time diagram that after discharging process was over, the concentration of bulk solution did not return to its original level. This indicates salt trapped in PEDOT:PSS layer. The reason for this phenomenon could be counter ions combined tightly with PEDOT:PSS via charge transfer during charging process. Our discharging process is zero voltage discharge, which only allows part of salt ions that was not tightly combined with PEDOT:PSS to diffuse back to bulk. A reverse voltage discharge (apply reverse voltage on electrodes) would help improve the reversibility of the desalination cycle.

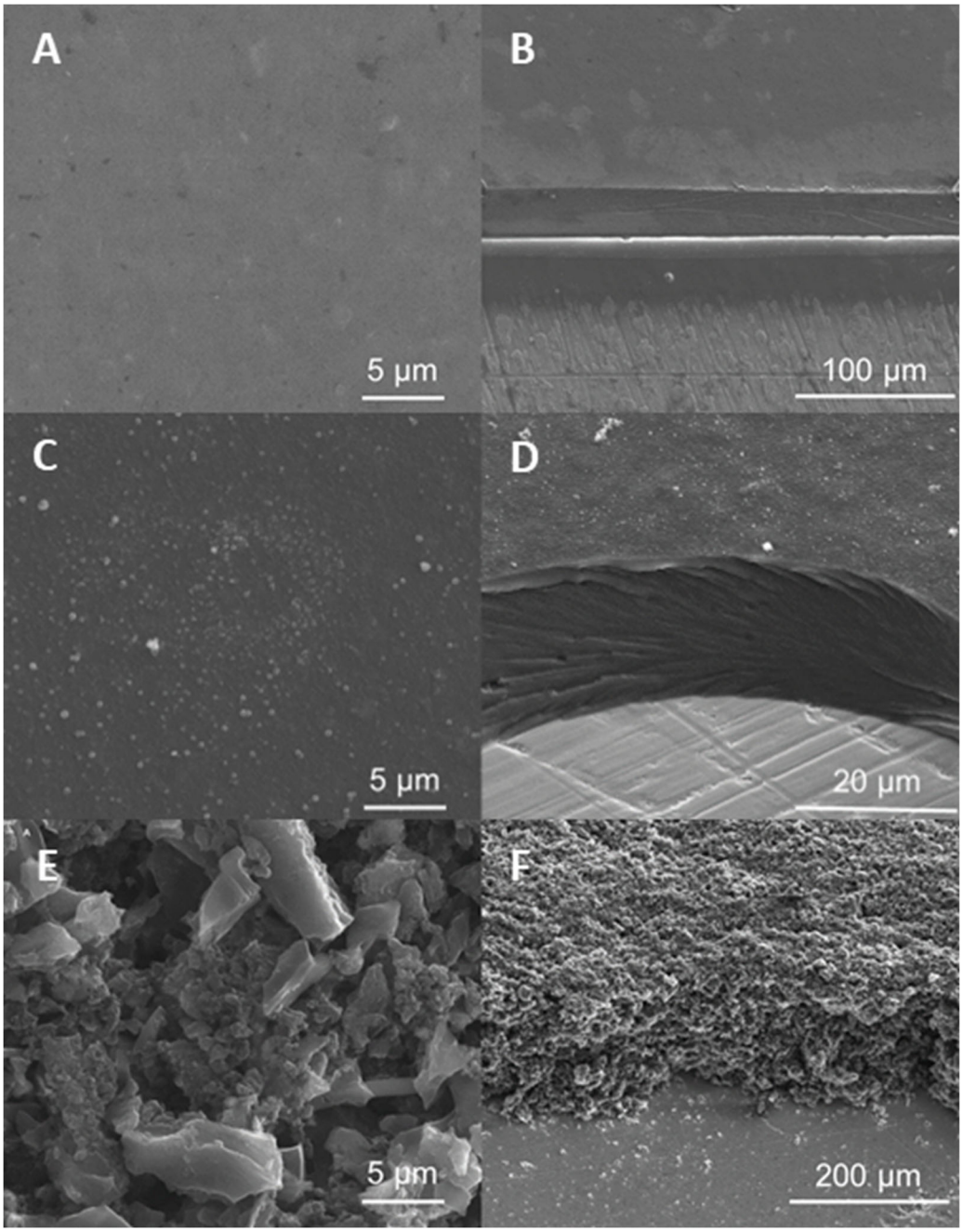

Figure 3.3 **SEM images of pristine PEDOT:PSS, surface treated PEDOT:PSS, and activated carbon**
Pristine PEDOT:PSS (A) top view (B) cross section; Surface treated PEDOT:PSS (C) top view (D) cross section; Activated carbon (E) top view (F) cross section

Figure 3.3 shows electron microscope images of the untreated PEDOT:PSS films (A and B) as well as the treated PEDOT:PSS film (C and D). For comparison, films of activated carbon are shown in E and F. Comparing to the pristine PEDOT:PSS surface

from our PEDOT:PSS procedure, surface treatment steps we applied in this study obviously roughened the surface of PEDOT:PSS. Sulfuric acid treatment is also known to remove an amount of PSS component and make the conformation of PEDOT molecular chain to be more linear.[85] According to the cross section images (**Figure 3.3B, D, F**), the PEDOT:PSS films were approximately 25 microns in thickness, while thickness of activated carbon films are around 200 microns.

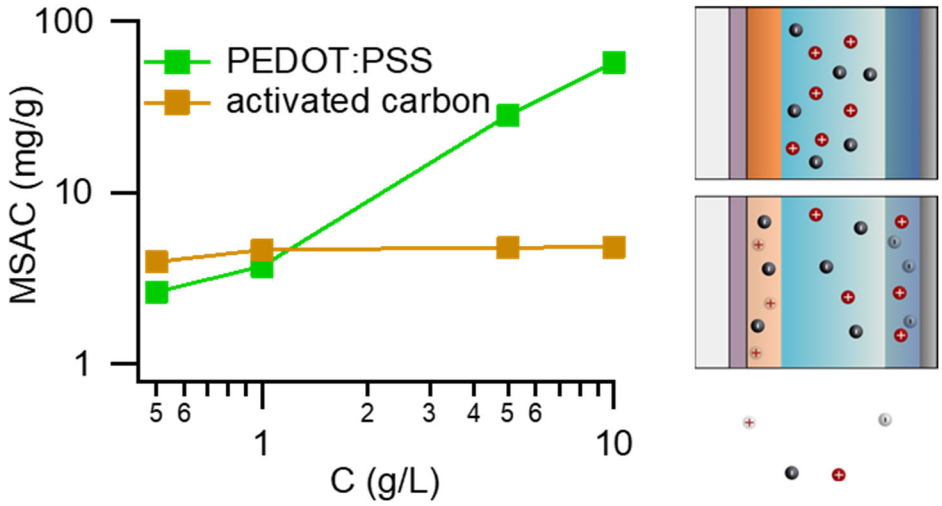

Figure 3.4 MSAC of activated carbon and PEDOT:PSS in different feed water concentrations

The MSAC of a desalinating electrode is the preferred metric for comparing between materials, as it is not affected by experimental conditions like film thickness or charging time. **Figure 3.4** shows the comparison between MSAC of CDI cell with PEDOT:PSS electrodes and activated carbon electrodes. It is important to point out that our activated carbon films are made with a simple recipe, and not highly optimized. **Figure 3.4** provides a clearer demonstration of the dissimilarity of these two materials, with the MSAC of PEDOT:PSS behaving linearly and the MSAC of activated carbon being approximately independent of concentration.

In a manner wholly dissimilar to activated carbon, the MSAC of PEDOT:PSS increases linearly with concentration. This can be interpreted as reflective of LeChatelier's principle, or more rigorously as a manifestation of Donnan equilibrium, known to determine the concentration dependent charging behavior of PEDOT:PSS films. When PEDOT:PSS charged with a negative potential, there would be more PSS carrying a negative charge able to combine with Na^+. While Cl^- passively adsorbed in the other half cell of

PEDOT:PSS CDI system, there would be more PEDOT carrying positive charge to combine with Cl^-. **Equation 3.1** is a half-cell reaction equation of our PEDOT:PSS CDI cell according to LeChatelier's principle. Since PEDOT:PSS electrode is solid, [PSS-] is not changing, when feed water NaCl concentration increases, the equilibrium will right shift, more NaCl will be attracted to the electrodes and combine with active PEDOT and PSS, and [Na:PSS] is proportion to [Na+] while k is a constant.

$$k[Na+][PSS-] \rightleftharpoons [Na{:}PSS] \qquad \textbf{3.1}$$

This behavior clearly demonstrates that the charging of PEDOT:PSS is not best described with double layer charging models common to materials like activated carbon. Rather, the fundamental charging process appears Faradaic, redox reactions between electrodes and counter-ions caused by charge transfer is the mechanism of desalination. The SAC of Faradaic electrodes is not restricted by electrode surface area, this also explains the superior performance of PEDOT:PSS over activated carbon. In addition, the technological implications of this behavior warrant further comment. The observed increase in SAC with salt concentration is likely not specific to PEDOT:PSS, as ion incorporation into other polymers is frequently described in terms of Faradaic processes, hinting that conducting polymers can be used to efficiently desalinate feed water streams of higher salinity.

The ability of PEDOT:PSS to function as both the cation collecting and anion collecting electrode is unusual. It is known that PEDOT:PSS typically only transports cations,[87,88] with the reduction of PEDOT:PSS being modulated by cation inclusion and the oxidation of PEDOT:PSS being modulated by cation expulsion. However, our observation of capacitive deionization requires both cation and anion transport into the film. The solution must remain charge balanced, thus the SAC of the film requires the transport of both ions from bulk to electrodes. It is known that Ag/AgCl electrode is also a well studied faradaic electrode, while our configuration contains an Ag/AgCl wire as reference electrode. To figure out whether Ag/AgCl reference electrode interferes the measurement, simple test was done by substituting the anion collecting PEDOT:PSS electrode with bare titanium current collector. The result turns out removing the anion collecting PEDOT:PSS electrode does not allow for capacitive deionization, which eliminates any considerations that the other 5 electrodes in the cell meaningfully contribute

to the observed SAC. Moreover, the linear increase in MSAC with increasing solution concentration is not observed in activated carbon, which further demonstrates that the other components of our coin cell do not meaningfully contribute to the observed MSAC.

In summary, conductive polymers are promising candidates for next-generation water deionization technologies, as demonstrated here with PEDOT:PSS. In order to achieve deionization in PEDOT:PSS, it had to be forced to transport anions. This was achieved by treatment with $CaCl_2$. The films can achieve an MSAC of over 55 mg/g which could likely be improved with further optimization. The MSAC of PEDOT:PSS shows a very different relationship with respect to solution concentration than does activated carbon, demonstrating that the former is charged via a Faradaic process while the latter relies on an electrostatic double layer charging mechanism.

Chapter 4. Future work

We have demonstrated the potential of PEDOT:PSS being next generation CDI electrodes with our developed in-situ CDI performance test system. However, there are always spaces for improvement to make more accurate performance test with our system. Ag/AgCl wire have been used in the CDI cell setup as the reference electrode to control the applied potential on two CDI electrodes accurately and individually. But, during a long desalination test after salt adsorption on CDI electrodes reached MSAC for a while (~10 min), white particles were observed to form on the electrode which the reduction took place (**Figure 4.1B**). This process can be observed on solution conductivity measurement reading due to ground shifting (**Figure 4.1A**). Need to notice that white particle only deposits on negative electrode when electrodes are not able to adsorb more counter ions in electrolyte. Perera and Rosenstein et.al. have explained the mechanism of Ag nanoparticle deposition on negative potential electrode (**Figure 4.1C**).[89] Although many studies includes Ag/AgCl reference electrode between CDI electrodes to control applied potential,[90–92] a better reference electrode would improve the stability of long desalination test. Hu et.al. have applied a PdH_x reference electrode for determining performance of hybrid CDI cell with activated carbon electrode and graphene oxide-CNT composite electrode, demonstrated PdH_x as a stable reference electrode that can be applied to CDI performance determination.[93]

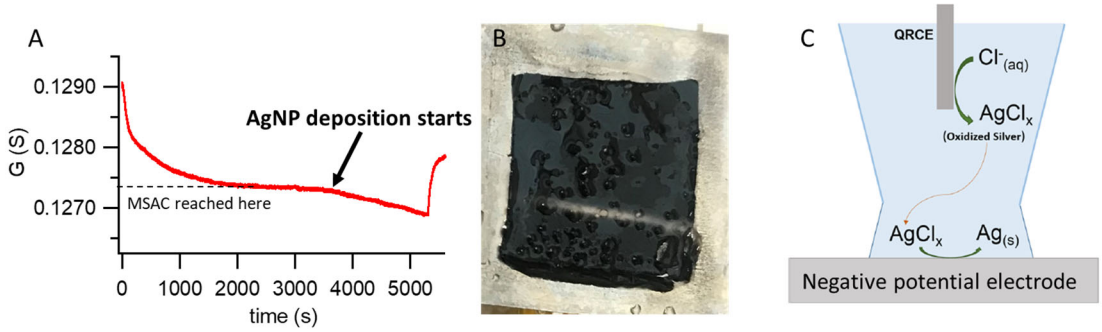

Figure 4.1 (A) After electrodes reached MSAC for 600 seconds AgNP deposition happened (B) AgNP formed on the negative electrode (C) Mechanism of AgNP formation according to Perera and Rosenstein et.al.[89]

Based on the desalination performance of PEDOT:PSS, high performance CDI system with optimized PEDOT:PSS as electrode would also be a direction of this project. In order to achieve a better CDI performance with PEDOT:PSS, one of the methods is to

build a hybrid CDI cell with a better Cl^- adsorber. Example have been mentioned in the introduction chapter, PSQ implanted with $[Fe(CN)_6]^{4-}$ is an excellent Cl^- adsorber,[73] which could have been utilized as positive electrode in our hybrid CDI system. Another method is to build a flow CDI system with PEDOT:PSS dispersion. Since flow CDI has demonstrated continuous desalination of wide range of feed water concentration, it is feasible to apply water soluble PEDOT:PSS as flow electrode in flow CDI system. However, the conductivity of PEDOT:PSS water dispersion might not be easy to control, which can be a challenge of this application.

Besides CDI technique, the ion selectivity of PEDOT:PSS is also worth to study. It has been reported that PEDOT:PSS as ion exchange membrane have high selectivity on Ca^{2+} over Na^+.[35] Surface treatments or polymer chain modifications can be done to allow PEDOT:PSS to have higher selectivity to other ions, such as Li^+. This might be an interesting project not only for providing technical support for mining lithium from ocean, but also for inspiring new generation high-capacity lithium battery.

References

(1) Sampa. *English: Global Water Consumption 1900-2025, by Region, in Billions M3 per Year.*; 2018. https://commons.wikimedia.org/wiki/File:Annualglobalwaterconsumption.jpg (accessed 2022-12-19).

(2) Gleick, P. H. Water as a Weapon and Casualty of Conflict: Freshwater and International Humanitarian Law. *Water Resour. Manag.* **2019**, *33* (5), 1737–1751. https://doi.org/10.1007/s11269-019-02212-z.

(3) *2017 State of the climate: Mountain glaciers | NOAA Climate.gov*. http://www.climate.gov/news-features/featured-images/2017-state-climate-mountain-glaciers (accessed 2022-09-18).

(4) *Advances in Water Desalination*; Lior, N., Ed.; Wiley series on advances in water desalination; Wiley, a John Wiley & Sons, Inc. Publication: Hoboken, New Jersey, 2013.

(5) Jones, E.; Qadir, M.; van Vliet, M. T. H.; Smakhtin, V.; Kang, S. The State of Desalination and Brine Production: A Global Outlook. *Sci. Total Environ.* **2019**, *657*, 1343–1356. https://doi.org/10.1016/j.scitotenv.2018.12.076.

(6) Miller, J. *Review of Water Resources and Desalination Technologies*; SAND2003-0800, 809106; 2003; pp SAND2003-0800, 809106. https://doi.org/10.2172/809106.

(7) Farhadi, F.; Deymi-Dashtebayaz, M.; Tayyeban, E. Studying a Multi-Stage Flash Brine Recirculation (MSF-BR) System Based on Energy, Exergy and Exergoeconomic Analysis. *Water* **2022**, *14* (19), 3108. https://doi.org/10.3390/w14193108.

(8) Thu, K.; Ng, K. C.; Saha, B. B.; Koyama, S. Operational Strategy of Adsorption Desalination Systems. *Int. J. Heat Mass Transf.* **2009**, *52* (7–8), 1811–1816. https://doi.org/10.1016/j.ijheatmasstransfer.2008.10.012.

(9) Fritzmann, C.; Löwenberg, J.; Wintgens, T.; Melin, T. State-of-the-Art of Reverse Osmosis Desalination. *Desalination* **2007**, *216* (1–3), 1–76. https://doi.org/10.1016/j.desal.2006.12.009.

(10) Lee, K. P.; Arnot, T. C.; Mattia, D. A Review of Reverse Osmosis Membrane Materials for Desalination—Development to Date and Future Potential. *J. Membr. Sci.* **2011**, *370* (1–2), 1–22. https://doi.org/10.1016/j.memsci.2010.12.036.

(11) Greenlee, L. F.; Lawler, D. F.; Freeman, B. D.; Marrot, B.; Moulin, P. Reverse Osmosis Desalination: Water Sources, Technology, and Today's Challenges. *Water Res.* **2009**, *43* (9), 2317–2348. https://doi.org/10.1016/j.watres.2009.03.010.

(12) Qasim, M.; Badrelzaman, M.; Darwish, N. N.; Darwish, N. A.; Hilal, N. Reverse Osmosis Desalination: A State-of-the-Art Review. *Desalination* **2019**, *459*, 59–104. https://doi.org/10.1016/j.desal.2019.02.008.

(13) Curto, D.; Franzitta, V.; Guercio, A. A Review of the Water Desalination Technologies. *Appl. Sci.* **2021**, *11* (2), 670. https://doi.org/10.3390/app11020670.

(14) Han, L.; Liu, Y.; Chew, J. W. Boron Transfer during Desalination by Electrodialysis. *J. Membr. Sci.* **2018**, *547*, 64–72. https://doi.org/10.1016/j.memsci.2017.10.036.

(15) Al-Amshawee, S.; Yunus, M. Y. B. M.; Azoddein, A. A. M.; Hassell, D. G.; Dakhil, I. H.; Hasan, H. A. Electrodialysis Desalination for Water and Wastewater: A Review. *Chem. Eng. J.* **2020**, *380*, 122231. https://doi.org/10.1016/j.cej.2019.122231.

(16) Mir, N.; Bicer, Y. Integration of Electrodialysis with Renewable Energy Sources for Sustainable Freshwater Production: A Review. *J. Environ. Manage.* **2021**, *289*, 112496. https://doi.org/10.1016/j.jenvman.2021.112496.

(17) *ESTPURE. "A chemical wastewater reuse and quality promotion project in Shanxi."* https://web.archive.org/web/20131203014753/http://estpure.com/a/cases/detail_62.aspx (accessed 2022-12-19).

(18) Liu, E.; Lee, L. Y.; Ong, S. L.; Ng, H. Y. Treatment of Industrial Brine Using Capacitive Deionization (CDI) towards Zero Liquid Discharge – Challenges and Optimization. *Water Res.* **2020**, *183*, 116059. https://doi.org/10.1016/j.watres.2020.116059.

(19) Helmholtz, H. Ueber einige Gesetze der Vertheilung elektrischer Ströme in körperlichen Leitern mit Anwendung auf die thierisch-elektrischen Versuche. *Ann. Phys. Chem.* **1853**, *165* (6), 211–233. https://doi.org/10.1002/andp.18531650603.

(20) Shapovalov, V. L.; Brezesinski, G. Breakdown of the Gouy−Chapman Model for Highly Charged Langmuir Monolayers: Counterion Size Effect. *J. Phys. Chem. B* **2006**, *110* (20), 10032–10040. https://doi.org/10.1021/jp056801b.

(21) Stern, O. Zur Theorie Der Elektrolytischen Doppelschicht. *Z. Für Elektrochem. Angew. Phys. Chem.* **1924**, *30* (21–22), 508–516. https://doi.org/10.1002/bbpc.192400182.

(22) Brown, M. A.; Goel, A.; Abbas, Z. Effect of Electrolyte Concentration on the Stern Layer Thickness at a Charged Interface. *Angew. Chem.* **2016**, *128* (11), 3854–3858. https://doi.org/10.1002/ange.201512025.

(23) BLAIR, J. W.; MURPHY, G. W. Electrochemical Demineralization of Water with Porous Electrodes of Large Surface Area. In *SALINE WATER CONVERSION*; Advances in Chemistry; American Chemical Society, 1960; Vol. 27, pp 206–223. https://doi.org/10.1021/ba-1960-0027.ch020.

(24) Farmer, J. C.; Fix, D. V.; Mack, G. V.; Pekala, R. W.; Poco, J. F. Capacitive Deionization of NaCl and NaNO3 Solutions with Carbon Aerogel Electrodes. *J. Electrochem. Soc.* **1996**, *143* (1), 159–169. https://doi.org/10.1149/1.1836402.

(25) Johnson, A. M.; Newman, J. Desalting by Means of Porous Carbon Electrodes. *J. Electrochem. Soc.* **1971**, *118* (3), 510–517. https://doi.org/10.1149/1.2408094.

(26) Farmer, J. C.; Fix, D. V.; Mack, G. V.; Pekala, R. W.; Poco, J. F. Capacitive Deionization of NH4CIO4 Solutions with Carbon Aerogel Electrodes. 12.

(27) Suss, M. E.; Porada, S.; Sun, X.; Biesheuvel, P. M.; Yoon, J.; Presser, V. Water Desalination via Capacitive Deionization: What Is It and What Can We Expect from It? *Energy Environ. Sci.* **2015**, *8* (8), 2296–2319. https://doi.org/10.1039/C5EE00519A.

(28) Zhao, R.; Biesheuvel, P. M.; van der Wal, A. Energy Consumption and Constant Current Operation in Membrane Capacitive Deionization. *Energy Environ. Sci.* **2012**, *5* (11), 9520. https://doi.org/10.1039/c2ee21737f.

(29) Porada, S.; Zhao, R.; van der Wal, A.; Presser, V.; Biesheuvel, P. M. Review on the Science and Technology of Water Desalination by Capacitive Deionization. *Prog. Mater. Sci.* **2013**, *58* (8), 1388–1442. https://doi.org/10.1016/j.pmatsci.2013.03.005.

(30) Johnson, A. M.; VENOLIA, W. The Electrosorb Process for Desalting Water. **1970**.

(31) Suss, M. E.; Baumann, T. F.; Bourcier, W. L.; Spadaccini, C. M.; Rose, K. A.; Santiago, J. G.; Stadermann, M. Capacitive Desalination with Flow-through Electrodes. *Energy Environ. Sci.* **2012**, *5* (11), 9511–9519. https://doi.org/10.1039/C2EE21498A.

(32) Remillard, E. M.; Shocron, A. N.; Rahill, J.; Suss, M. E.; Vecitis, C. D. A Direct Comparison of Flow-by and Flow-through Capacitive Deionization. *Desalination* **2018**, *444*, 169–177. https://doi.org/10.1016/j.desal.2018.01.018.

(33) Folaranmi, G.; Bechelany, M.; Sistat, P.; Cretin, M.; Zaviska, F. Towards Electrochemical Water Desalination Techniques: A Review on Capacitive Deionization, Membrane Capacitive Deionization and Flow Capacitive Deionization. *Membranes* **2020**, *10* (5), 96. https://doi.org/10.3390/membranes10050096.

(34) Hassanvand, A.; Chen, G. Q.; Webley, P. A.; Kentish, S. E. An Investigation of the Impact of Fouling Agents in Capacitive and Membrane Capacitive Deionisation. *Desalination* **2019**, *457*, 96–102. https://doi.org/10.1016/j.desal.2019.01.031.

(35) Nnorom, N. C.; Rogers, T.; Jain, A.; Alazmi, A.; Elias, W. C.; DuChanois, R. M.; Flores, K.; Gardea-Torresdey, J. L.; Cokar, M.; Elimelech, M.; Wong, M. S.; Verduzco, R. Sulfonated Polymer Coating Enhances Selective Removal of Calcium in Membrane

Capacitive Deionization. *J. Membr. Sci.* **2022**, *662*, 120974. https://doi.org/10.1016/j.memsci.2022.120974.

(36) Yu, F.; Yang, Z.; Cheng, Y.; Xing, S.; Wang, Y.; Ma, J. A Comprehensive Review on Flow-Electrode Capacitive Deionization: Design, Active Material and Environmental Application. *Sep. Purif. Technol.* **2022**, *281*, 119870. https://doi.org/10.1016/j.seppur.2021.119870.

(37) Jeon, S.; Park, H.; Yeo, J.; Yang, S.; Cho, C. H.; Han, M. H.; Kim, D. K. Desalination via a New Membrane Capacitive Deionization Process Utilizing Flow-Electrodes. *Energy Environ. Sci.* **2013**, *6* (5), 1471. https://doi.org/10.1039/c3ee24443a.

(38) Jeon, S.; Yeo, J.; Yang, S.; Choi, J.; Kim, D. K. Ion Storage and Energy Recovery of a Flow-Electrode Capacitive Deionization Process. *J. Mater. Chem. A* **2014**, *2* (18), 6378. https://doi.org/10.1039/c4ta00377b.

(39) Suss, M. E.; Presser, V. Water Desalination with Energy Storage Electrode Materials. *Joule* **2018**, *2* (1), 10–15. https://doi.org/10.1016/j.joule.2017.12.010.

(40) Oladunni, J.; Zain, J. H.; Hai, A.; Banat, F.; Bharath, G.; Alhseinat, E. A Comprehensive Review on Recently Developed Carbon Based Nanocomposites for Capacitive Deionization: From Theory to Practice. *Sep. Purif. Technol.* **2018**, *207*, 291–320. https://doi.org/10.1016/j.seppur.2018.06.046.

(41) Hou, C.-H.; Huang, C.-Y. A Comparative Study of Electrosorption Selectivity of Ions by Activated Carbon Electrodes in Capacitive Deionization. *Desalination* **2013**, *314*, 124–129. https://doi.org/10.1016/j.desal.2012.12.029.

(42) Han, B.; Cheng, G.; Wang, Y.; Wang, X. Structure and Functionality Design of Novel Carbon and Faradaic Electrode Materials for High-Performance Capacitive Deionization. *Chem. Eng. J.* **2019**, *360*, 364–384. https://doi.org/10.1016/j.cej.2018.11.236.

(43) Han, L.; Karthikeyan, K. G.; Anderson, M. A.; Gregory, K. B. Exploring the Impact of Pore Size Distribution on the Performance of Carbon Electrodes for Capacitive

Deionization. *J. Colloid Interface Sci.* **2014**, *430*, 93–99. https://doi.org/10.1016/j.jcis.2014.05.015.

(44) Porada, S.; Weinstein, L.; Dash, R.; van der Wal, A.; Bryjak, M.; Gogotsi, Y.; Biesheuvel, P. M. Water Desalination Using Capacitive Deionization with Microporous Carbon Electrodes. *ACS Appl. Mater. Interfaces* **2012**, *4* (3), 1194–1199. https://doi.org/10.1021/am201683j.

(45) Zou, L.; Li, L.; Song, H.; Morris, G. Using Mesoporous Carbon Electrodes for Brackish Water Desalination. *Water Res.* **2008**, *42* (8–9), 2340–2348. https://doi.org/10.1016/j.watres.2007.12.022.

(46) Baroud, T. N.; Giannelis, E. P. High Salt Capacity and High Removal Rate Capacitive Deionization Enabled by Hierarchical Porous Carbons. *Carbon* **2018**, *139*, 614–625. https://doi.org/10.1016/j.carbon.2018.05.053.

(47) Wang, H.; Yuan, X.; Wu, Y.; Huang, H.; Peng, X.; Zeng, G.; Zhong, H.; Liang, J.; Ren, M. Graphene-Based Materials: Fabrication, Characterization and Application for the Decontamination of Wastewater and Wastegas and Hydrogen Storage/Generation. *Adv. Colloid Interface Sci.* **2013**, *195–196*, 19–40. https://doi.org/10.1016/j.cis.2013.03.009.

(48) Gu, X.; Hu, M.; Du, Z.; Huang, J.; Wang, C. Fabrication of Mesoporous Graphene Electrodes with Enhanced Capacitive Deionization. *Electrochimica Acta* **2015**, *182*, 183–191. https://doi.org/10.1016/j.electacta.2015.09.076.

(49) Biswas, C.; Lee, Y. H. Graphene Versus Carbon Nanotubes in Electronic Devices. *Adv. Funct. Mater.* **2011**, *21* (20), 3806–3826. https://doi.org/10.1002/adfm.201101241.

(50) Li, H.; Pan, L.; Lu, T.; Zhan, Y.; Nie, C.; Sun, Z. A Comparative Study on Electrosorptive Behavior of Carbon Nanotubes and Graphene for Capacitive Deionization. *J. Electroanal. Chem.* **2011**, *653* (1–2), 40–44. https://doi.org/10.1016/j.jelechem.2011.01.012.

(51) Zhao, J.; Wang, Z.; White, J. C.; Xing, B. Graphene in the Aquatic Environment: Adsorption, Dispersion, Toxicity and Transformation. *Environ. Sci. Technol.* **2014**, *48* (17), 9995–10009. https://doi.org/10.1021/es5022679.

(52) Shi, W.; Li, H.; Cao, X.; Leong, Z. Y.; Zhang, J.; Chen, T.; Zhang, H.; Yang, H. Y. Ultrahigh Performance of Novel Capacitive Deionization Electrodes Based on A Three-Dimensional Graphene Architecture with Nanopores. *Sci. Rep.* **2016**, *6* (1), 18966. https://doi.org/10.1038/srep18966.

(53) Zhang, S.; Wang, Y.; Han, X.; Cai, Y.; Xu, S. Optimizing the Fabrication of Carbon Nanotube Electrode for Effective Capacitive Deionization via Electrophoretic Deposition Strategy. *Prog. Nat. Sci. Mater. Int.* **2018**, *28* (2), 251–257. https://doi.org/10.1016/j.pnsc.2018.02.010.

(54) Jia, B.; Zhang, W. Preparation and Application of Electrodes in Capacitive Deionization (CDI): A State-of-Art Review. *Nanoscale Res. Lett.* **2016**, *11* (1), 64. https://doi.org/10.1186/s11671-016-1284-1.

(55) Li, Y.; Qi, J.; Li, J.; Shen, J.; Liu, Y.; Sun, X.; Shen, J.; Han, W.; Wang, L. Nitrogen-Doped Hollow Mesoporous Carbon Spheres for Efficient Water Desalination by Capacitive Deionization. *ACS Sustain. Chem. Eng.* **2017**, *5* (8), 6635–6644. https://doi.org/10.1021/acssuschemeng.7b00884.

(56) Yasin, A. S.; Jeong, J.; Mohamed, I. M. A.; Park, C. H.; Kim, C. S. Fabrication of N-Doped &SnO2-Incorporated Activated Carbon to Enhance Desalination and Bio-Decontamination Performance for Capacitive Deionization. *J. Alloys Compd.* **2017**, *729*, 764–775. https://doi.org/10.1016/j.jallcom.2017.09.185.

(57) Min, X.; Hu, X.; Li, X.; Wang, H.; Yang, W. Synergistic Effect of Nitrogen, Sulfur-Codoping on Porous Carbon Nanosheets as Highly Efficient Electrodes for Capacitive Deionization. *J. Colloid Interface Sci.* **2019**, *550*, 147–158. https://doi.org/10.1016/j.jcis.2019.04.082.

(58) Li, Q.; Zheng, Y.; Xiao, D.; Or, T.; Gao, R.; Li, Z.; Feng, M.; Shui, L.; Zhou, G.; Wang, X.; Chen, Z. Faradaic Electrodes Open a New Era for Capacitive Deionization. *Adv. Sci.* **2020**, *7* (22), 2002213. https://doi.org/10.1002/advs.202002213.

(59) Chen, F.; Huang, Y.; Guo, L.; Sun, L.; Wang, Y.; Yang, H. Y. Dual-Ions Electrochemical Deionization: A Desalination Generator. *Energy Environ. Sci.* **2017**, *10* (10), 2081–2089. https://doi.org/10.1039/C7EE00855D.

(60) Yuan, S.; Liu, Y.-B.; Xu, D.; Ma, D.-L.; Wang, S.; Yang, X.-H.; Cao, Z.-Y.; Zhang, X.-B. Pure Single-Crystalline $Na_{1.1}V_3O_{7.9}$ Nanobelts as Superior Cathode Materials for Rechargeable Sodium-Ion Batteries. *Adv. Sci.* **2015**, *2* (3), 1400018. https://doi.org/10.1002/advs.201400018.

(61) Bao, W.; Tang, X.; Guo, X.; Choi, S.; Wang, C.; Gogotsi, Y.; Wang, G. Porous Cryo-Dried MXene for Efficient Capacitive Deionization. *Joule* **2018**, *2* (4), 778–787. https://doi.org/10.1016/j.joule.2018.02.018.

(62) Cao, J.; Wang, Y.; Wang, L.; Yu, F.; Ma, J. $Na_3V_2(PO_4)_3$@C as Faradaic Electrodes in Capacitive Deionization for High-Performance Desalination. *Nano Lett.* **2019**, *19* (2), 823–828. https://doi.org/10.1021/acs.nanolett.8b04006.

(63) Byles, B. W.; Hayes-Oberst, B.; Pomerantseva, E. Ion Removal Performance, Structural/Compositional Dynamics, and Electrochemical Stability of Layered Manganese Oxide Electrodes in Hybrid Capacitive Deionization. *ACS Appl. Mater. Interfaces* **2018**, *10* (38), 32313–32322. https://doi.org/10.1021/acsami.8b09638.

(64) Tang, Y.; Zhang, Y.; Li, W.; Ma, B.; Chen, X. Rational Material Design for Ultrafast Rechargeable Lithium-Ion Batteries. *Chem. Soc. Rev.* **2015**, *44* (17), 5926–5940. https://doi.org/10.1039/C4CS00442F.

(65) Nam, D.-H.; Choi, K.-S. Electrochemical Desalination Using Bi/BiOCl Electrodialysis Cells. *ACS Sustain. Chem. Eng.* **2018**, *6* (11), 15455–15462. https://doi.org/10.1021/acssuschemeng.8b03906.

(66) Li, Y.; Ding, Z.; Li, J.; Li, J.; Lu, T.; Pan, L. Highly Efficient and Stable Desalination via Novel Hybrid Capacitive Deionization with Redox-Active Polyimide Cathode. *Desalination* **2019**, *469*, 114098. https://doi.org/10.1016/j.desal.2019.114098.

(67) Wu, Y.; Zeng, R.; Nan, J.; Shu, D.; Qiu, Y.; Chou, S.-L. Quinone Electrode Materials for Rechargeable Lithium/Sodium Ion Batteries. *Adv. Energy Mater.* **2017**, *7* (24), 1700278. https://doi.org/10.1002/aenm.201700278.

(68) Zhao, Q.; Whittaker, A.; Zhao, X. Polymer Electrode Materials for Sodium-Ion Batteries. *Materials* **2018**, *11* (12), 2567. https://doi.org/10.3390/ma11122567.

(69) Kong, H.; Yang, M.; Miao, Y.; Zhao, X. Polypyrrole as a Novel Chloride-Storage Electrode for Seawater Desalination. *Energy Technol.* **2019**, *7* (11), 1900835. https://doi.org/10.1002/ente.201900835.

(70) Wang, Y.; Han, X.; Wang, R.; Xu, S.; Wang, J. Preparation Optimization on the Coating-Type Polypyrrole/Carbon Nanotube Composite Electrode for Capacitive Deionization. *Electrochimica Acta* **2015**, *182*, 81–88. https://doi.org/10.1016/j.electacta.2015.09.020.

(71) Wang, Y.; Wang, R.; Xu, S.; Liu, Q.; Wang, J. Polypyrrole/Polyaniline Composites with Enhanced Performance for Capacitive Deionization. *Desalination Water Treat.* **2015**, *54* (12), 3248–3256. https://doi.org/10.1080/19443994.2014.907748.

(72) Zhu, L.; Shen, Y.; Sun, M.; Qian, J.; Cao, Y.; Ai, X.; Yang, H. Self-Doped Polypyrrole with Ionizable Sodium Sulfonate as a Renewable Cathode Material for Sodium Ion Batteries. *Chem. Commun.* **2013**, *49* (97), 11370. https://doi.org/10.1039/c3cc46642f.

(73) Silambarasan, K.; Joseph, J. Redox-Polysilsesquioxane Film as a New Chloride Storage Electrode for Desalination Batteries. **2019**, 8.

(74) Sakunpongpitiporn, P.; Phasuksom, K.; Paradee, N.; Sirivat, A. Facile Synthesis of Highly Conductive PEDOT:PSS via Surfactant Templates. *RSC Adv.* **2019**, *9* (11), 6363–6378. https://doi.org/10.1039/C8RA08801B.

(75) Dauzon, E.; Lin, Y.; Faber, H.; Yengel, E.; Sallenave, X.; Plesse, C.; Goubard, F.; Amassian, A.; Anthopoulos, T. D. Stretchable and Transparent Conductive PEDOT:PSS-Based Electrodes for Organic Photovoltaics and Strain Sensors Applications. *Adv. Funct. Mater.* **2020**, *30* (28), 2001251. https://doi.org/10.1002/adfm.202001251.

(76) Wen, N.; Fan, Z.; Yang, S.; Zhao, Y.; Cong, T.; Xu, S.; Zhang, H.; Wang, J.; Huang, H.; Li, C.; Pan, L. Highly Conductive, Ultra-Flexible and Continuously Processable PEDOT:PSS Fibers with High Thermoelectric Properties for Wearable Energy Harvesting. *Nano Energy* **2020**, *78*, 105361. https://doi.org/10.1016/j.nanoen.2020.105361.

(77) Kumar, S.; Umar, M.; Saifi, A.; Kumar, S.; Augustine, S.; Srivastava, S.; Malhotra, B. D. Electrochemical Paper Based Cancer Biosensor Using Iron Oxide Nanoparticles Decorated PEDOT:PSS. *Anal. Chim. Acta* **2019**, *1056*, 135–145. https://doi.org/10.1016/j.aca.2018.12.053.

(78) Fuller, E. J.; Keene, S. T.; Melianas, A.; Wang, Z.; Agarwal, S.; Li, Y.; Tuchman, Y.; James, C. D.; Marinella, M. J.; Yang, J. J.; Salleo, A.; Talin, A. A. Parallel Programming of an Ionic Floating-Gate Memory Array for Scalable Neuromorphic Computing. **2019**, 6.

(79) Stöcker, T.; Köhler, A.; Moos, R. Why Does the Electrical Conductivity in PEDOT:PSS Decrease with PSS Content? A Study Combining Thermoelectric Measurements with Impedance Spectroscopy. *J. Polym. Sci. Part B Polym. Phys.* **2012**, *50* (14), 976–983. https://doi.org/10.1002/polb.23089.

(80) AFG1022 Arbitrary Function Generator Programmer Manual.

(81) *AFG3000 Series Quick Start User Manual*. https://download.tek.com/manual/071164002.pdf (accessed 2022-12-20).

(82) *MODEL SR810 DSP Lock-In Amplifier user manual*. https://www.thinksrs.com/downloads/pdfs/manuals/SR810m.pdf (accessed 2022-12-20).

(83) Bandarenka, A. S. Exploring the Interfaces between Metal Electrodes and Aqueous Electrolytes with Electrochemical Impedance Spectroscopy. *The Analyst* **2013**, *138* (19), 5540. https://doi.org/10.1039/c3an00791j.

(84) Inoue, A.; Yuk, H.; Lu, B.; Zhao, X. Strong Adhesion of Wet Conducting Polymers on Diverse Substrates. *Sci. Adv.* **2020**, *6* (12), eaay5394. https://doi.org/10.1126/sciadv.aay5394.

(85) Kumar, S. R. S.; Kurra, N.; Alshareef, H. N. Enhanced High Temperature Thermoelectric Response of Sulphuric Acid Treated Conducting Polymer Thin Films. *J. Mater. Chem. C* **2016**, *4* (1), 215–221. https://doi.org/10.1039/C5TC03145A.

(86) Zhao, R.; Satpradit, O.; Rijnaarts, H. H. M.; Biesheuvel, P. M.; van der Wal, A. Optimization of Salt Adsorption Rate in Membrane Capacitive Deionization. *Water Res.* **2013**, *47* (5), 1941–1952. https://doi.org/10.1016/j.watres.2013.01.025.

(87) Volkov, A. V.; Wijeratne, K.; Mitraka, E.; Ail, U.; Zhao, D.; Tybrandt, K.; Andreasen, J. W.; Berggren, M.; Crispin, X.; Zozoulenko, I. V. Understanding the Capacitance of PEDOT:PSS. *Adv. Funct. Mater.* **2017**, *27* (28), 1700329. https://doi.org/10.1002/adfm.201700329.

(88) Rebetez, G.; Bardagot, O.; Affolter, J.; Réhault, J.; Banerji, N. What Drives the Kinetics and Doping Level in the Electrochemical Reactions of PEDOT:PSS? *Adv. Funct. Mater.* **2022**, *32* (5), 2105821. https://doi.org/10.1002/adfm.202105821.

(89) Perera, R. T.; Rosenstein, J. K. Quasi-Reference Electrodes in Confined Electrochemical Cells Can Result in in Situ Production of Metallic Nanoparticles. *Sci. Rep.* **2018**, *8* (1), 1965. https://doi.org/10.1038/s41598-018-20412-2.

(90) Holubowitch, N.; Omosebi, A.; Gao, X.; Landon, J.; Liu, K. Quasi-Steady-State Polarization Reveals the Interplay of Capacitive and Faradaic Processes in Capacitive Deionization. *ChemElectroChem* **2017**, *4* (9), 2404–2413. https://doi.org/10.1002/celc.201700082.

(91) Avraham, E.; Noked, M.; Cohen, I.; Soffer, A.; Aurbach, D. The Dependence of the Desalination Performance in Capacitive Deionization Processes on the Electrodes PZC. *J. Electrochem. Soc.* **2011**, *158* (12), P168. https://doi.org/10.1149/2.078112jes.

(92) Tang, W.; He, D.; Zhang, C.; Kovalsky, P.; Waite, T. D. Comparison of Faradaic Reactions in Capacitive Deionization (CDI) and Membrane Capacitive Deionization (MCDI) Water Treatment Processes. *Water Res.* **2017**, *120*, 229–237. https://doi.org/10.1016/j.watres.2017.05.009.

(93) Hu, C.-C.; Hsieh, C.-F.; Chen, Y.-J.; Liu, C.-F. How to Achieve the Optimal Performance of Capacitive Deionization and Inverted-Capacitive Deionization. *Desalination* **2018**, *442*, 89–98. https://doi.org/10.1016/j.desal.2018.05.013.